A HEART IN THE HAND: 3D PRINTED MODELS OF CONGENITAL HEART DEFECTS OPTIMIZED FOR TEACHING

by
Laura S. Roy

A thesis submitted to Johns Hopkins University in conformity with the requirements for the degree of Master of Arts

Baltimore, Maryland
March, 2016

ABSTRACT

Almost 1% of U.S. births are affected by congenital heart defects (CHDs). Understanding CHDs is critical for families to make sense of risks and benefits of treatment. Cardiac spatial complexity makes 3D models an important teaching aid, and 3D printed cardiovascular models featuring CHDs have educational promise due to anatomical faithfulness; reproducibility; material color, transparency and flexibility; and scalability (an important consideration with infant anatomy). New technology has opened up opportunities to recreate anatomy from CT, MRI, and echocardiography data and produce models with unprecedented detail. Some research facilities are creating 3D printed models of CHDs, but the current focus in the field is on pre-surgical planning with patient education as an ancillary goal. Understanding CHDs on a traditional heart model is very difficult for clinicians, and even more so for emotionally-strained families lacking a sound background in anatomy, who may have only a few minutes with a cardiac expert.

The focus of this research was to determine the best workflow to develop 3D printed models with CHDs optimized for educating patients and patient families. The research explores new technologies in 3D printing to create didactic 3D printed cardiovascular models featuring CHDs.

The 3D printed and digital models resulting from this research were produced using Horos®, ZBrush®, and Photoshop® based on pediatric patient cardiovascular CT scans. The digital models were scaled up in size to permit easier viewing of anatomical detail. Multiple printers and a variety of materials were used to produce prototype models. The resulting 3D printed models are anatomically faithful and strategically simplified to focus attention on areas of interest. Color was used didactically and with consideration for the target audience of patient families. The end result of this research was establishment of a workflow protocol for producing didactic 3D printed cardiovascular prints. This workflow has potential to be adapted for other anatomical structures such as the cerebral vasculature or hepatic portal system, and for other audiences such as medical students and trainees.

Author: Laura S. Roy

CHAIRPERSONS OF THE SUPERVISORY COMMITTEE

Preceptor:	**Duke Cameron, M.D**., Chief of Cardiac Surgery, Johns Hopkins Hospital
Faculty Advisor:	**Gary Lees, M.S., C.M.I., F.A.M.I.**, Chair of the Department of Art as Applied to Medicine, Johns Hopkins University School of Medicine
Secondary Faculty Advisor:	**Juan Garcia, M.A., C.C.A.**, Associate Professor of the Department of Art as Applied to Medicine, Johns Hopkins University School of Medicine

ACKNOWLEDGMENTS

Thanks to Dr. Duke Cameron, Chief of Cardiac Surgery at Johns Hopkins Hospital, for serving as my preceptor, and for his time, extensive expertise, critical anatomical review, encouragement, and insights. Thanks to Gary Lees, Chair of the Department of Art as Applied to Medicine at Johns Hopkins School of Medicine, for serving as my faculty advisor, for organizing funding, for his guidance and critique, and for his great outlook that kept the project moving forward. He was there to keep me going when I got frustrated and to celebrate with me when I had success. Thanks to Juan Garcia, my secondary advisor and Associate Professor of the Department of Art as Applied to Medicine at Johns Hopkins School of Medicine, for his 3D printing and medical sculpting expertise, his tireless efforts to help me advance the project, and his help challenging me out of my comfort zone to work effectively and collaboratively.

Thanks to Dr. Luca Vricella, Director of Pediatric Heart Transplantation at Johns Hopkins Hospital, who provided critical feedback and enthusiasm toward this project, and to Dr. Naru Hibino, for his imaging review session and consultation on 3D printing. I would also like to thank Dr. Stefan Zimmerman for his enthusiasm and help in selection of anatomical data files. Thanks to Richard Curtis from Adobe® for spending time instructing me on new techniques and to CJ Stein from Stratasys Direct® who worked with me to get successful 3D prints. I also greatly appreciate the support of the Vesalius Trust, for their grant to help fund this project.

Thanks to Amy, Caitlin, Emily, Erica, Kai-ou, and Kari, as well as the classes of ‘14 and ‘16, for encouraging me to do my best and for inspiring me through their own endeavors. Thanks to the Department of Art as Applied to Medicine faculty for their expertise, good spirits, and critical feedback. I am inspired by each of you in a unique way that I will always remember. Thanks to John Dorn and to Dean Biechler for the inspiration to focus on what I love in illustration and to stick with it through the long hours.

Thank you to my amazing love Jeremy for his endless support, encouragement, constructive critique of mechanics and aesthetics, and delicious cooking. Special thank you to my sister Katy for all of the late-night editing. Thanks to Mom, Dad, Ben, Elizabeth, and the rest of my family and friends, for their love and support throughout my life and education.

TABLE OF CONTENTS

FIGURES

INTRODUCTION

Congenital cardiovascular defects, also known as congenital heart defects (CHDs), are problems in the heart that are present from birth. CHDs are caused by incorrect formation of the heart, the cardiac vasculature, or the cardiac conduction system. They may have a genetic or environmental basis. In the United States, 0.8% of births are affected by CHDs (Pye and Green, 2003) (about 40,000 births annually), and CHDs are responsible for twice as many childhood deaths as all cancers combined (CDC, 2016a). About 25% of CHD births are affected by "critical" CHDs which require surgical intervention within about the first year (CDC, 2016a).

Cardiac spatial complexity makes 3D models an important teaching aid, and 3D printed cardiovascular models featuring CHDs have educational promise due to the potential for anatomical faithfulness; reproducibility; material color, transparency, and flexibility; and scalability (an important consideration with infant anatomy). New technology has opened up opportunities to recreate anatomy from CT, MRI, and echocardiography data and to produce models with unprecedented detail. Some research facilities are producing 3D printed models of CHDs, but the current focus in the field is on pre-surgical planning, with patient education as an ancillary goal. Understanding CHDs on a traditional heart model is very difficult for clinicians. It is more difficult for families lacking a sound background in anatomy and who may have only a few minutes with a cardiac expert, especially with the emotional level of decision-making and concerns about understanding the risks and benefits of treatment. The focus of this research was to determine the best workflow to create 3D printed cardiovascular models with CHDs optimized for educating patients and patient families using real imaging data.

CONGENITAL HEART DEFECTS

CHDs comprise a range of heart problems. Defects can be described in terms of affected blood flow as cyanotic, acyanotic, or obstructive. Cyanotic lesions cause an overall shunting of blood from right to left, resulting in less oxygenation of the blood. The most common forms of cyanotic lesions are tetralogy of Fallot, transposition of the great arteries, truncus arteriosus, total anomalous pulmonary venous connection, and tricuspid atresia (Sesler, 2012). Shunting of blood from left to right, on the other hand, is known as an acyanotic condition. Atrial septal defects are the most common acyanotic lesion (Noel and Lewin, 2012). An obstructive defect causes blockage of blood, such as may be caused by narrowing of vessels. Coarctation of the aorta and pulmonary stenosis are examples of obstructive defects (Schulz, 2012). For a list of CHDs, see Appendix A.

IMAGING OF CHDS

Computed tomography (CT), magnetic resonance imaging (MRI), and echocardiography ("echo") are each used to visualize the heart in patients. CT imaging is the method of taking a series of cross-sectional radiographic images ("slices"). MRI uses a similar process by taking cross-sectional image slices based on magnetized water particles. Echo is a form of ultrasound that uses sound waves to bounce off structures which can then be interpreted as 2D or 3D data.

CT and MRI images can be viewed as the original slices or in a variety of reconstructed 2D or 3D views, allowing the viewer to learn information about the inside of an object without cutting into to it. The slices can be further reconstructed as individual 3D structures through a process called segmentation, wherein the boundaries of a structure are defined on individual slices, and a volume is created from the restricted data. For example, the 2D boundary of a vessel can be traced on multiple slices and mapped into 3D space. The space between slices is extrapolated to fill in the missing information.

Important imaging considerations include resolution and duration. Resolution determines how much information must be extrapolated by the image viewing software over a defined distance. CT and MRI slices taken at greater distances apart will require the computer to fill in more information versus slices taken at lesser distances apart which can generate a relatively more detailed and accurate 3D volume reconstruction.

Duration of a scan can affect precision of boundaries. If the subject is moving, the scan may document the subject in different positions and result in blurred images or displaced structures. The faster the scan, the less likely these distortions will be significant. This is of particular importance in a structure that is always moving, such as the heart. The beating heart is in constant movement, so the same scan could capture a crisp image of the ribs and a fuzzy or blurred image of the heart. A traditional adult CT scan may take anywhere from 15-60 minutes (St. Michael's, 2016). Each minute, an adult heart typically beats 60-100 times, and an infant heart typically beats 80-160 times (RNCeus, 2016). To clearly view the heart of an infant, a high-speed scan and/or echo must be used. Recent developments in CT have made it possible to scan an infant chest in roughly 0.2 seconds, which would be the elapsed time of about 1/3 of a heartbeat. The faster scan will yield a less blurred image than the traditional scan, although the amount of movement in 1/3 of a heartbeat (roughly one systole or diastole event) will still show some motion blur. Echo is better for visualizing valves and sections of the heart.

EXISTING EDUCATIONAL CHD RESOURCES

Educational print and web resources are widely available for CHDs. Many hospitals and heart associations have websites with text descriptions, 2D illustrations, and sometimes simple animations. Examples of websites with significant educational resources on the subject include those of the American Heart Association®; the Congenital Heart Information Network; Cove Point Foundation; and Little Hearts Inc. A Google® search for even the rarer of CHDs, such as double chamber right ventricle or congenitally corrected transposition of the great arteries, will yield a variety of visual resources. A doctor may supply a brochure with basic information and illustrations from a publisher like Krames Patient Education. Illustrated books are also available, including *The Parent's Guide to Children's Congenital Heart Defects*, by Gerri Kramer and Shari Maurer, and *The Heart of a Child*, by Catherine Neill.

Interactive digital applications aimed toward patient education are increasing in the medical field and some are focused

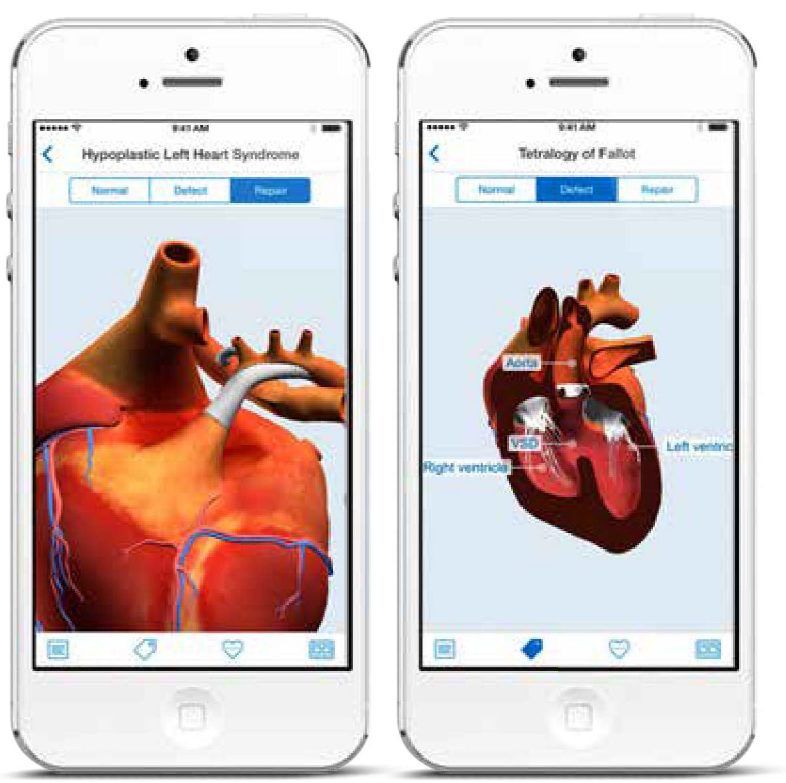

Fig. 1-1: Heartpedia screenshots (Cincinnati Children's, 2016) (text not intended to be read)

on CHD education. Notably, Cincinnati Children's Hospital released the *Heartpedia* app for iPad, iPhone, and Android in 2014 (Fig. 1-1). As of the writing of this thesis, the app is free and features 12 hearts with congenital defects. App users can compare normal to defective and surgically corrected anatomy in whole or sectioned hearts. Additional detailed textual descriptions and animations are also included.

The Multimedia Atlas of Congenital Heart Diseases (Fig. 1-2), released in 2012, is available on DVD. It presents animations on 11 CHDs, focusing on morphology, pathophysiology, clinical aspects, diagnosis, medical therapy, and surgical therapy. The atlas is suitable to guide families, but its primary audience is clinicians and medical students.

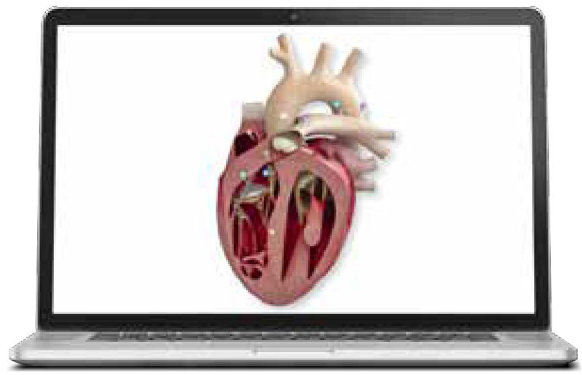

Fig. 1-2: Heart image from The Multimedia Atlas of Congenital Heart Diseases (Al Medica Italia, 2012)

The 3D Road Map to Congenital Heart Disease (Fig. 1-3), first released in 2014 by Dahku Creations for PC and iPad, focuses on enhancing teaching techniques by use of didactic color and graphics. This app is promoted as suitable for any interested audience, and is therefore not optimized for any particular audience.

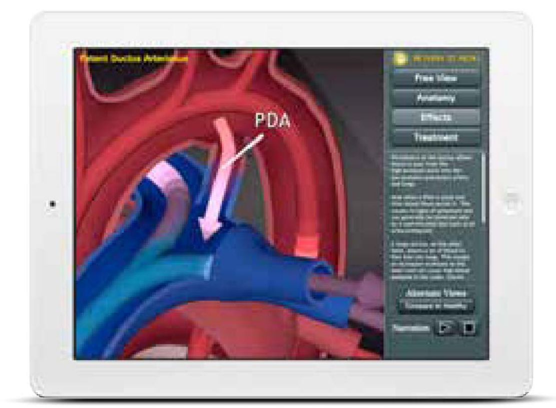

Fig. 1-3: The 3D Road Map to Congenital Heart Disease screenshots (Dahku Creations, 2015) (text not intended to be read)

Each of these computer apps uses stylized hearts which are not closely based on any particular patient's anatomy. More anatomically-realistic resources exist for medical professionals, but they are not well-adapted for a lay audience.

The University College London (UCL) has created a *Library of 3D Anatomies* (Fig. 1-4). As opposed to the app resources described above, UCL's virtual library features patient-specific anatomical models obtained through CT, MRI, and echocardiography. The UCL library contains images and interactive 3D models of CHDs as well as acquired heart defects and other non-cardiovascular anatomical features. They are not available for download.

Some tangible 3D CHD models exist, including 3D printed versions. British company Adam,Rouilly Ltd. is the only company the author has found to offer 3D anatomical models of CHDs (Fig. 1-5). The company offers models for four defects. Design hierarchy is based on applying cutaways to reveal CHD anatomy adjusted from a single idealized heart. As a set, this "small multiple" approach makes differences easy to distinguish and didactically effective, but overall anatomical realism is understated (e.g. there is no evidence of the characteristic "boot shape" in the tetralogy of Fallot model). Valves and muscle texture are prominently featured, and didactic color (red and blue) generally indicates the level of oxygenation in the blood vessels. These models would be most useful with a specialist to guide the learning experience. Normal heart anatomical models are available from sources such as Adam,Rouilly Ltd. and Laerdl. High quality anatomical models are often handmade and/or hand-painted, leading to significant production costs.

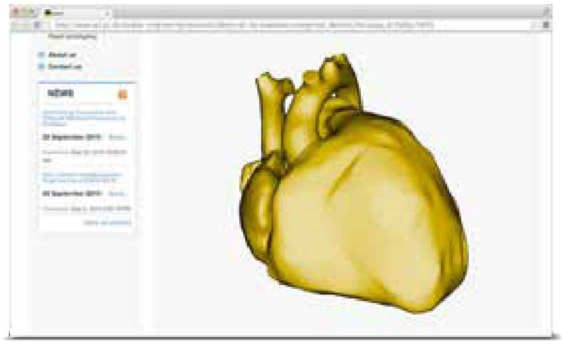

Fig. 1-4: Tetralogy of Fallot model from UCL Library of 3D Anatomies (2016) (text not intended to be read)

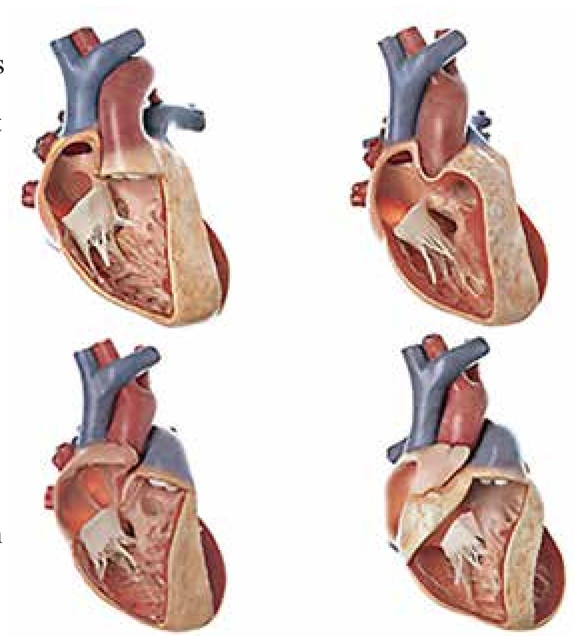

Fig. 1-5: Models of CHDs (Adam,Rouilly Ltd., 2010). Clockwise from top left: transposition of the great arteries, tetralogy of Fallot, total atrioventricular canal, various defects of the ventricular septum

Some 3D printed CHDs are available for teaching patients. Materialise® can be contracted to make patient-specific 3D prints, and they offer some of those for sale through their HeartPrint® and HeartPrint Flex® series (Fig. 1-6). They offer a variety of didactic approaches such as printing negative spaces in multiple colors based on anatomical location or combining transparent and opaque structures. They also print in a translucent flexible material. Materialise is currently increasing their available prints. These can be excellent teaching and planning tools for medical

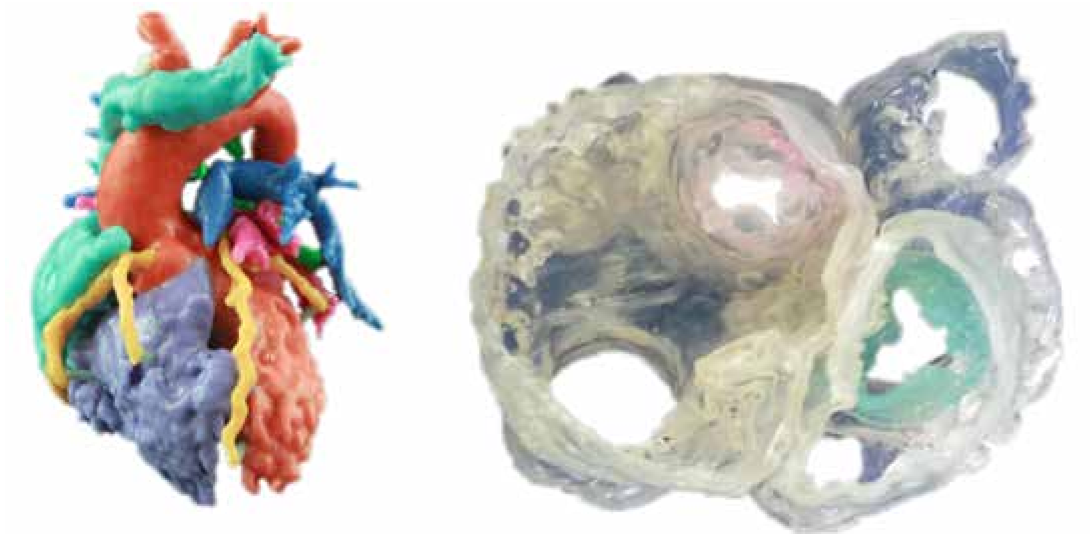

Fig. 1-6: 3D-printed CHD models. Left: HeartPrint® in ColorJet technology; right: HeartPrint® in HeartPrint® Flex materials. (Materialise, 2016)

professionals, but the prints are not optimized for a lay audience due to overuse or underuse of didactic color, unnecessary detail, and lack of hierarchy. Many families can learn to read these models, but it involves an unnecessary amount of education to convey the relevant concepts.

PATIENT FAMILIES

CHDs are almost always identified prenatally or in the infant patient, so parents and families are responsible for considering physician advice and making care decisions. Awareness of the child's condition causes parents and family to be emotionally affected at the time of diagnosis. About 15% of CHDs are detected prenatally (CDC, 2016b). Some CHDs are predicted by genetic analysis. In cases where CHDs are diagnosed prenatally, parents have some time to consider treatment options should the pregnancy come to term. Otherwise, patients are not diagnosed until after birth. Parents often have at best several months to consider treatment decisions, or at worst a matter of days or hours. This leads to a great deal of stress and often inadequate time to understand the patient's condition or to carefully consider medical decisions (Smith, 2011).

Parents each respond to the situation uniquely, but they may experience a range of emotions, including shock, disbelief, fear, blame, anger, and sadness (Pye and Green, 2003) which conflicts with the joy associated with becoming a parent (Clark, 1999). Guilt may also accompany the necessity of choosing a treatment that will have a lifelong effect on the child (Smith, 2011). Despite the fact that medical intervention is continually improving, survival rate and quality of life of patients can be limited; even with early treatment some children with CHDs will require a heart transplant later in life, and some will not survive at all (Pye and Green, 2003). Studies of parents of children with CHDs indicate that they experience more stress than parents of children with other chronic illness due to the immediate potential for an unsuccessful outcome (Clark, 1999), and an "overwhelming feeling of helplessness" is reported by most families following a CHD diagnosis (Smith, 2011).

These conflicting and overwhelming emotions can seriously impair a parent who needs to understand the medical situation of the child in order to make an informed treatment decision.

3D PRINTING

3D printing is an umbrella term encompassing many types of additive manufacturing processes. Alternately known as rapid prototyping (RP), direct digital manufacturing (DDM), and layered manufacturing, 3D printing is a suite of technologies decreasing in cost as they advance in capability to produce models in a variety of materials, textures, colors, and size. The technology of 3D printing was invented in the early 1980s when Hideo Kodama invented the technique known now as stereolithography, which involves curing layers of photopolymers with ultraviolet lasers to build up three-dimensional objects. Chuck Hull of 3D Systems Corporation patented his process for stereolithography in 1984 and contributed the stereolithography (.stl) file format that has become the basis for many 3D printing technologies.

As technology advances, 3D printing is becoming a more viable option for producing educational models versus traditional casting or handcrafting techniques because it allows for prototyping of multiple model iterations to test and determine effectiveness without committing to a large production run. Scale, color, material, and didactic emphasis can be adjusted and tested with focus groups before committing to a design, and the design need never be "final." Neither a mold nor production line are needed, so a change in design only requires the cost of design development. 3D printed models are customizable, reproducible, and scalable—an important factor in educational models. For example, a typical newborn heart is about 3.5cm square, or the size of a walnut. Scaling up in size, even by an order of 50-100%, can aid significantly in anatomical visibility. The quality of 3D printing is now satisfactory for both prototype and final product production and can often be translated to large-scale production lines if desired.

3D PRINTING TECHNIQUES

3D printing requires a digital model that is without holes, or "watertight," for the printer to define printing boundaries. All polygons must have consistent normals (they must all be facing either outwards or inwards) to prevent printer confusion. Each printer has specific requirements, such as limitations of wall thickness, size, complexity, and need for extra supports. Major types of 3D printing technologies are listed below, followed by brief descriptions.

- ColorJet Printing (CJP, also known as Z-Corp or Zprinter)
- Digital Light Processing (DLP)
- Electron Beam Melting (EBM)
- Fused Deposition Modeling (FDM) and Fused Filament Fabrication (FFF)
- Laminated Object Manufacturing (LOM)
- PolyJet Printing
- Selective Laser Sintering (SLS)
- Selective Laser Melting (SLM)
- Stereolithography (SLA)

ColorJet Printing (CJP) is produced by thinly spreading a layer of powdered material over a build surface. Corresponding to color and volume data of a 3D digital file, a layer of color and binder is selectively applied to the powder. More powder is spread over the previous layer and the process is repeated until a part is fully built. CJP is an excellent resource for quickly producing full-color prototypes. A drawback is the grainy surface and fragility associated with this type of printing, although material durability is improving. This and other powder-based 3D printing technologies have an advantage of requiring no external supports, which makes printing of complex geometry and overhangs easy; the powder itself acts as a support. At the end of the process, the finished 3D print is removed from the unfused powder.

Digital Light Processing (DLP) uses liquid plastic photopolymer that is hardened using UV light. The light is directed using small mirrors aimed through a projection lens. The UV light quickly hardens each layer of resin, resulting in excellent resolution with low cost and low waste. DLP is a process similar to stereolithography, but its system of lighting is different. It typically uses arc lamps. This printing technology is well-suited for small, intricate work like jewelry design, hearing aids, or dental applications.

Electron Beam Melting (EBM) is used for metal part manufacture. It uses an electron beam aimed into a vacuum chamber. A layer of metal powder, such as titanium, is spread across the bed of the machine, and the electron beam selectively melts and fuses the print one layer at a time. EBM 3D printing manufacturers such as Sciaky® offer machines that can build large parts (up to 110” x 110” x 110” with their EBAM technology) suitable for aerospace and similar industries. For most industries, though, EBM is still fairly expensive so its use is limited (3DPrintingfromscratch.com, 2014).

Fused Deposition Modeling (FDM), invented by Stratasys®, is nearly identical to Fused Filament Fabrication (FFF), the technology used by many popular desktop printers. These technologies involve feeding a filament of thermoplastic into a heated extrusion head, which then deposits the heated material on a build platform one layer at a time. Print time is determined by the size and complexity of the object, layer thickness, and other printer settings. FDM/FFF require printing of additional support structures to facilitate printing of overhangs. The supports are removed after printing.

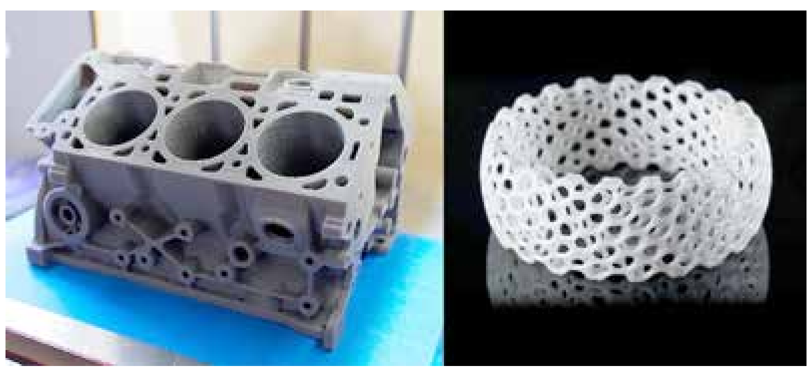

Fig. 1-7: Examples of FDM/FFF (3Dprintingfromscratch.com, 2016)

FDM/FFF is a popular technology for many reasons. It is available in affordable desktop models in addition to professional models. It can print in an environmentally-friendly way in a variety of materials—the most common being ABS (acrylonitrile butadiene styrene—the same material used to make Lego® bricks), PC (polycarbonate—used to make many products such as CDs, safety goggles, etc.), and PLA (polylactide—a biodegradable polyester), which are strong and as such are typically suitable for testing as part prototypes. It is a useful technology for concept design and prototyping, and some industries use it to produce end-use products—most often for small complex parts (Fig. 1-7).

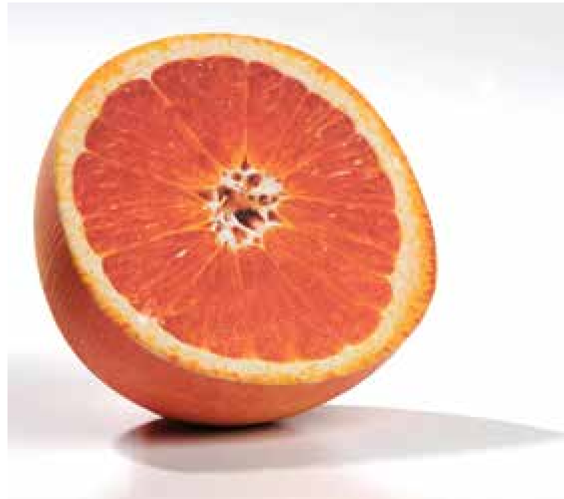
Fig. 1-8: LOM printed with layered paper (MCor technologies, 2016)

Laminated Object Manufacturing (LOM) is a process which layers, fuses, and shapes sheets of material. The material is typically paper, PVC plastic or metal sheets. The LOM process includes several steps. LOM printers use a continuous scroll of material coated with adhesive. The scroll is unrolled across the printing area where a piece is cut out with a knife or laser. The scroll rolls another layer of material over the first and the two layers are fused with a heated roller that is passed over the material sheet to melt the adhesive. The new layer is cut to size, and the process is repeated until the whole part has been built. The cost of materials for LOM is relatively low and the prints can be large. Full color prints can be made by integrating ink-jet printing on paper during the process (Fig. 1-8). LOM is not a very popular printing method, in part because no major 3D printing companies offer LOM printing on a per-part basis. Cubic Technologies® and MCor Technologies® are two brands that produce LOM printers.

PolyJet technology is a fast printing technology and arguably the most versatile. It involves depositing droplets of both supporting and structural materials on a build plate. The structural material is immediately cured with UV light and the support material is washed off after printing. PolyJet offers a wide variety of plastics and colors. Objet® printers by Stratasys use PolyJet, such as the Objet® Connex3, which allows for three materials to be used. This capability results in a wide variety of choices in color and flexibility in the same print. As of February 2016, Stratasys and Adobe® announced a partnership which allows printing of blended material objects as defined by Photoshop® to a Connex3 machine. Using this “Connex3/Adobe” technology, parts can be printed with gradients of materials and colors within the same print.

Selective Laser Sintering (SLS) is similar to EBM. Powdered material is distributed on a print bed and selectively heated to bind it. This is repeated for additional layers until the print is completely built. As opposed to EBM, which uses an electron beam, SLS uses a computer-directed laser. SLS can print with a variety of materials, making it a popular choice for customized products and concept designs.

Fig. 1-9: SLM printing (3Dprintingfromscratch.com, 2016b)

Selective Laser Melting (SLM) is a metal printing technique similar to SLS in that SLM uses lasers to fuse fine metal powder layer by layer (fig. 1.9). The difference is that the metal is fully melted in SLM (like in EBM), whereas it is fused but not fully melted in SLS. SLM is popular in the aerospace industry as well as for manufacturing and concept-development of some medical devices, implants, and prosthetics.

Stereolithography (SLA) is the oldest 3D printing technique. Like DLP, it starts with a liquid photopolymer resin which is exposed to UV light layer by layer to cure it. 3D Systems® Corporation advanced this technology in the 1980s and it continues to be widely used today. Formlabs® recently entered the market with a desktop version of SLA technology. As with DLP, SLA offers excellent resolution and works fairly quickly. Like FDM/FFF, it requires supports for complex overhanging geometry which must be removed after printing.

CURRENT USES OF 3D PRINTING IN MEDICINE AND MEDICAL EDUCATION

Use of 3D printing in medicine has been increasing. It has been demonstrated to assist in clinical diagnosis, pre-surgical planning and surgical guidance, according to Sun and Squelch (2015), who also note that personalized devices and stents have been successfully developed with 3D printing. In January of 2016, Japan announced that 3D printing of surgical planning models would be covered by health insurance (3ders.org, 2016), indicating increasing international acceptance of and interest in 3D print technologies in medicine. Many surgical specialties are using 3D printing to practice a surgery in advance. Dr. Ivan Mendez of the University of Saskatchewan elected to practice a procedure on a flexible printed brain (fig. 1-10) from patient imaging after his standard technique of practicing with computer simulations failed

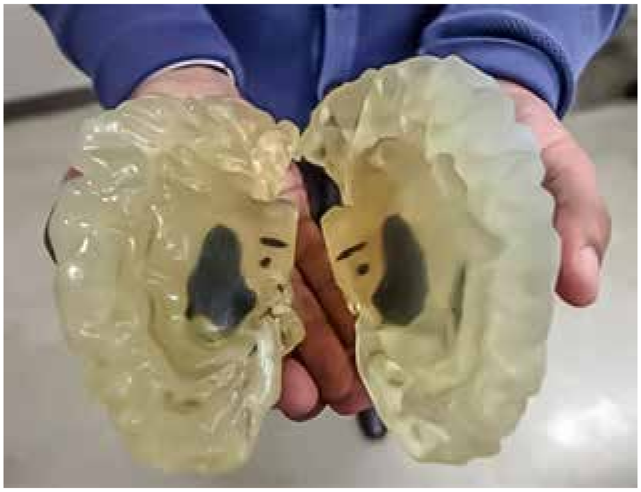

Fig. 1-10: Dr. Ivan Mendez with a 3D printed brain (3Ders.org, 2015c)

him (3Ders.org, 2015c). Other surgeons have used the technology to plan surgeries for brain aneurysms (3Ders.org, 2015a), heart surgery (3Ders.org, 2015ab), and tumors throughout the body.

The complexity of the cardiovascular system makes it well-suited for 3D printing. 3D printing of patient specific models is currently being used as a means of surgical planning to visualize and/or practice repair of tetralogy of Fallot and other CHDs, and its use has resulted in decreased surgical case time, operating room time, and 30-day readmission rate (Marsden and Feinstein, 2015).

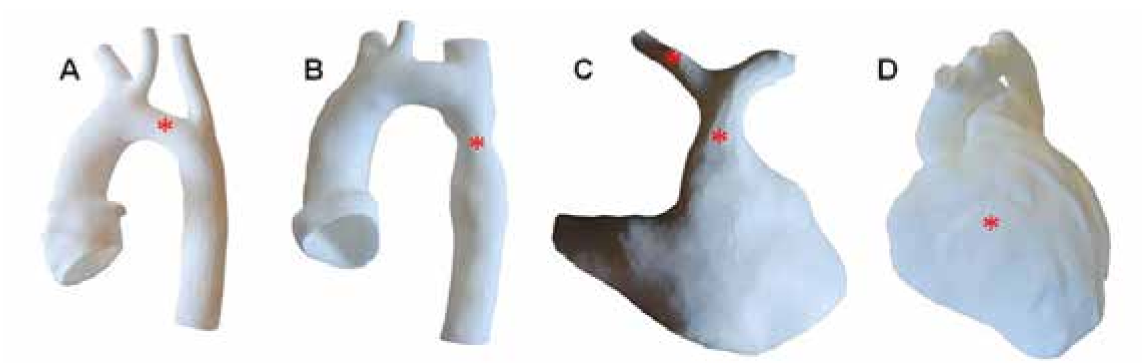

Fig. 1-11: Models used to educate parents about CHDs (Biglino et al, 2015) (text not intended to be read)

Some research has been done on use of 3D printed models of patient-specific anatomy for the purpose of communicating to parents about CHDs in their own children. Biglino et al (2015) found that parents were enthusiastic about the models, noting that:

> *"parent feedback highlighted that 3D models are perceived as more immediate and user-friendly than medical images... whose importance the parents recognized... but which they themselves found difficult to apprehend."*

Parents requested to keep the models in three quarters of cases.

Bernhard et al. (2016) conducted a study investigating effectiveness of educating patients with patient-specific kidney and tumor anatomy. Each 3D print (Fig. 1-12) was segmented from CT

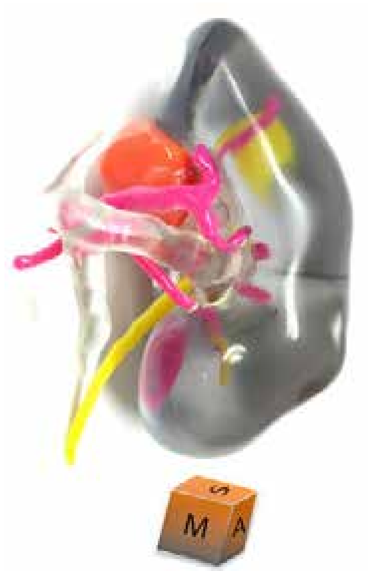

Fig. 1-12: Patient specific kidney model (Bernhard et al, 2016)

data and produced with PolyJet technology. Color was used didactically to show internal structures. Patients demonstrated improvement in understanding of basic kidney physiology, kidney anatomy, and tumor characteristics after interacting with their personal 3D kidney model, with the opportunity to ask questions of a physician.

Recent research by McMenamin et al. (2014) tested whether 3D printed replicas of human anatomy can serve as a substitute for cadaver dissection in gross anatomy education. They used ColorJet technology to reproduce anatomy using both surface scanning and CT scan data and found it to be an economical and rapid way to reproduce anatomical specimens.

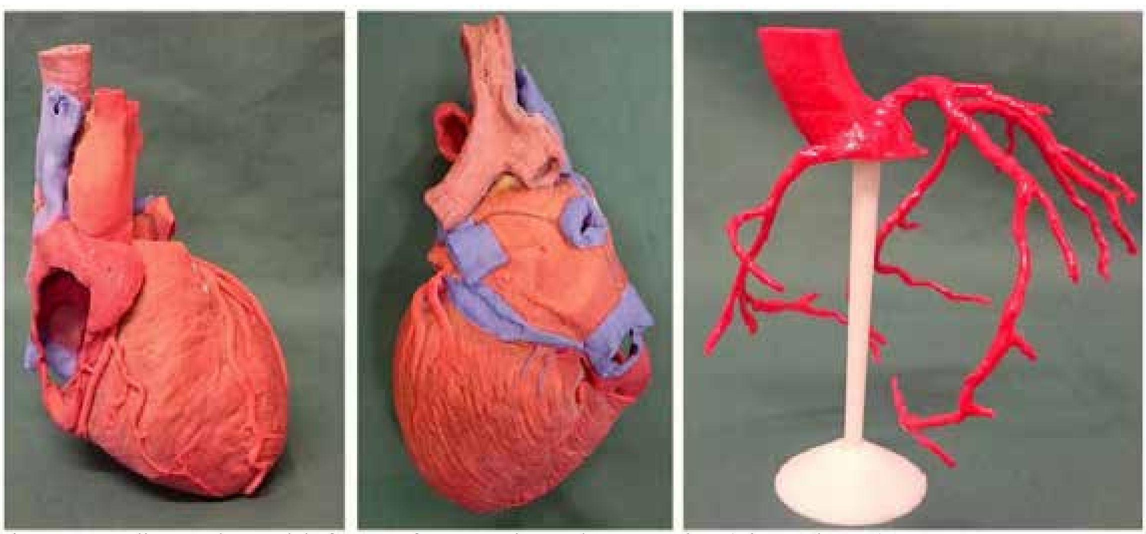

Fig. 1-13: Cardiovascular models from surface scanning and CT scan data (Lim et al, 2014)

Lim et al. (2015), using the protocol described by McMenamin et al (2014), produced cardiac models using CT and scan data from cadaveric hearts (Fig. 1-13). They provided student groups with access to either cadaveric hearts, 3D printed hearts, or a combination of the two materials and found significant improvement in post-test results of the group given *only* 3D printed hearts. They note limitations to their study but conclude that the 3D printed models were demonstrated to be associated with a statistically significant improvement in test scores and are thus suitable for supplementing a cadaver-based curriculum and exhibit several benefits over cadaver materials.

O’Reilly et al (2016) continued McMenamin and Lim’s line of investigation to produce a lower limb model and a femoral vessel access model using a combination of technologies. Lower limb bones were printed with ColorJet technology, as were molds to make silicone muscles using traditional casting techniques. The muscles were magnetized to the bones. The femoral access model for training students was produced with a novel workflow using 3D printing combined with traditional techniques to produce educational models

SHARING OF 3D PRINTABLE MODELS

Fig. 1-14: NIH 3D Print Exchange logo (Coakley, 2014)

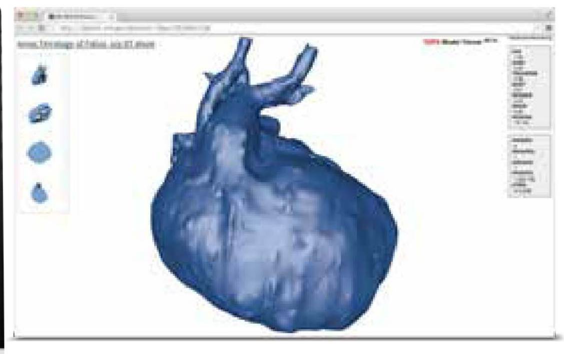

Fig. 1-15: Tetralogy of Fallot model on NIH 3D Print Exchange (text not intended to be read)

In mid-2014, the National Institutes of Health unveiled the 3D Print Exchange (fig. 1-14) as a means to coordinate sharing of “bioscientifically relevant 3D models suitable for 3D printing” (Coakley et al., 2014). The library contains a range of models from proteins and organs to prosthetics and custom lab ware, all of which can be downloaded and shared at no cost. Their heart library has several downloadable CHD 3D print files from patient data (fig. 1-15).

INTERACTIVE ELECTRONIC MEDIA

Use of interactive electronic media for education has increased as computers and mobile devices have become common in formal education, employment, and leisure environments. Apps are well-suited for educating the public about medical issues because they place information into a form that can be reviewed on demand. Multiple programs are available to produce and share animations as well as interactive 2D, 3D, and 4D content. Gaming engines like Unity offer extensive flexibility in tailoring the user experience with 3D objects and for producing interfaces to share animations. The expansion of web-based possibilities with the development of HTML5 has opened up many new teaching options, and programs for building interactive experiences based on HTML5 have great potential. Adobe® Edge Animate is well-suited for producing such content. JavaScript is another resource, and in particular three.js offers exciting new possibilities for integrating 3D models and experiences into HTML space.

Virtual reality is an exciting mode of visualization that has recently had a great deal of interest. YouTube® created a virtual reality channel in November of 2015. Content can be created for virtual reality in many compositing and 3D modeling programs, such as The Foundry's Nuke® and Maxon® Cinema 4D®. SketchFab® is a web-based 3D model and environment-sharing software that also has the option to support virtual reality by means of Google Cardboard®. First released in 2012, SketchFab was originally used primarily by video game developers, but it is now in use by many types of 3D artists and users/researchers who upload models produced by photogrammetry. SketchFab has the option to attach annotations and introduce animation in addition to giving users the ability to rotate and zoom in an object or environment. SketchFab in many ways replaces and improves the now defunct Quicktime® Virtual Reality file type (QTVR) which gave the experience of simple rotation around an object or within an environment. The Portable Document Format (PDF) also offers a 3D option, although it is more difficult to build into an interactive interface and is better suited for sharing isolated objects.

WHY A HEART IN THE HAND?

While 3D printed models are a relatively new teaching phenomenon, and there is still much to learn about their educational efficacy, studies have confirmed their usefulness in developing visuospatial understanding to a greater degree than textbooks and 3D computer models. A recent study demonstrated that a group of students using a 3D printed equine foot to learn its anatomy showed better visuospatial understanding and short-term retention than corresponding groups using textbooks or digital models (Preece et al, 2013). They speak specifically about the importance of 3D information in medical education. Rizzolo and Stewart's research into spatial learning by anatomy students (2006) supports this: "Tactile manipulation and the engagement of the multiple senses is considered one of the greatest advantages of cadaver dissection, and is believed to promote better understanding and retention of spatial information and relationships."

Like a bird in the hand is worth two in the bush, a heart in the hand can be worth several 2D hearts on a page. Parents have demonstrated a preference for tangible 3D models over illustrations when learning about CHDs (Biglino et al, 2015); yet, for most CHDs, no such resources exist. We now have the technology to use patient imaging as the basis for this undeveloped need.

The primary audience for this project is families who will see and use 3D printed cardiovascular models featuring CHDs at surgeon visits. To effectively teach parents and families of patients, educational materials should convey only the relevant information as quickly and clearly as possible. Additional understandable materials, such as an app corresponding to the 3D printed CHD models, should ideally be available to families while at home to supplement information from a consultation with the cardiologist or cardiac surgeon. Availability of the 3D printed models in a waiting area could further allow families to learn at their own pace.

The secondary audience is medical professionals with only a basic understanding of CHDs, such as medical students and radiologists/surgeons in training. Serving as an introduction to the subject, 3D printed CHDs could greatly improve understanding of surgical intervention for surgical residents. Radiology residents may benefit by using them to supplement training on how to interpret CHD imaging, which is difficult even with 3D images on a screen or in print.

MATERIALS AND METHODS

To create a 3D printed resource appropriate to teach about a CHD to parents, the following workflow was used (fig. 2-1). The process began by determining a didactic approach. Next, CT data was obtained, segmented, and converted to digital 3D models. The models were refined, optimized for teaching, 3D printed, and reviewed by cardiac surgeons and cardiologists. A way to integrate a supporting 2D mobile/web app resource was also explored.

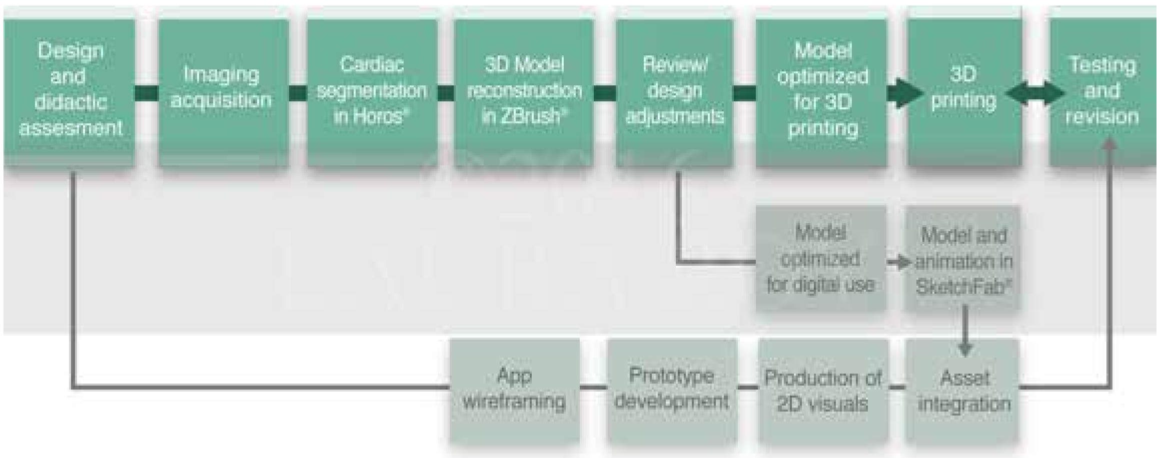

Fig. 2-1: Workflow summary to produce a didactic 3D printed CHD model and companion 2D application

DESIGN APPROACH

Basic guidelines were determined to guide development based on material restrictions of 3D printing techniques, didactic qualities, and feedback from cardiac surgeons. Colors were based on a red-blue scheme per the convention of oxygenated and de-oxygenated blood. Warm reds and warm blues were used when possible. It was decided to anatomically abbreviate CHD models to focus on relevant anatomy and downplay anatomy irrelevant to the particular CHD. Tangible 3D printed models would be sized to hold in the hand (roughly 7-10cm in any direction).

ColorJet printing was selected for full-color models. Slight color shift occurs as a result of the printing process, so a reference was used for color planning (PLANFAB, 2015) (fig. 2-2).

The Stratasys Objet Connex3 printers were selected for semi-full color models. Color options for the Connex3 at the time of writing include the rigid opaque materials cyan, magenta, yellow, white, black (“VeroCyan”, “VeroMagenta”, “VeroYellow”, “VeroWhite”, and “VeroBlack”); rigid clear (“VeroClear”); and the flexible translucent “TangoPlus” which could be mixed with rigid materials to produce a semi-flexible, semi-transparent colored materials. Color palettes chosen for use in this project are shown in fig. 2-3.

Fig. 2-2: Left: digital color swatches. Middle: color swatches printed on sandstone. Right: middle image with Protanopia type colorblind filter (PLANFAB, 2016). (Text not intended to be read)

Fig. 2-3: PolyJet Palettes used in this project. Left: VeroCyan/VeroMagenta/VeroYellow. Middle: VeroWhite/VeroCyan/VeroMagenta. Right: VeroMagenta/VeroCyan/TangoClear. (Text not intended to be read).

DATA ACQUISITION AND SELECTION

Computed tomography (CT) data was acquired from pediatric patients using the "free-breathing" high speed Siemens® Medical Systems SOMATOM® Force CT Scanner. Spatial resolution of the scans (distance between slices) was between .3mm and .75mm depending on the patient, and each scan took approximately 0.2s (fig. 2-4). The DICOM file format was used for storage

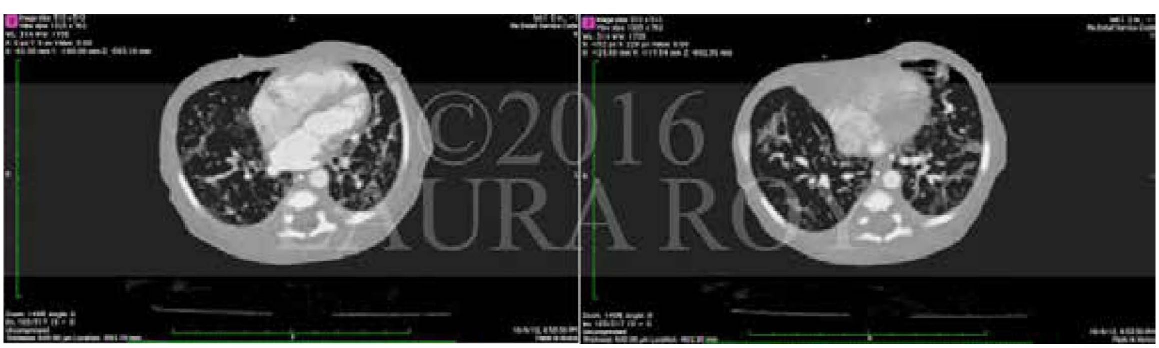

Fig. 2-4: CT slices from heart with tetralogy of Fallot defect. Left: mid-heart. Right: inferior heart. (Text not intended to be read)

of each set of scan data. CT scan data was collected for the following CHDs, which were pre-selected based on frequency of the CHD in the population and feedback from cardiac surgeons regarding difficulty of describing a condition to a family: atrial septal defect, ventricular septal defect, patent ductus arteriosus, coarctation of the aorta, tetralogy of Fallot, hypoplastic left heart syndrome, total anomalous pulmonary venous return, pulmonic stenosis, transposition of the great arteries, truncus arteriosus, aortic root aneurysm, and tricuspid atresia.

Upon reviewing the quality of the DICOM data and the preference of the cardiac surgeons, the list of defects for 3D prints was narrowed. Special consideration was given to spatial complexity and the difficulty to portray the defect without a 3D model. Candidates for 3D printed models within the scope of this thesis was limited to the following three CHDs:

- Tetralogy of Fallot
- Transposition of the great arteries (pre-operative and post-operative)
- Aortic root aneurysm (pre-operative and post-operative)

MASTER MODEL PRODUCTION

The model development process required isolation and segmentation of cardiac data from the DICOM image data. The internal surface of the heart (i.e., the solid blood pool, or the negative volume) and the external surface of the heart were segmented. The internal surface was deleted from the external surface with a Boolean operation to produce a hollow heart. Further processing was determined based on specific didactic needs of the CHD and included reconstruction in Pixologic® ZBrush® to smooth surfaces as well as to rebuild surfaces difficult to visualize from the CT. Reconstructed anatomy was produced based on anatomical landmarks in the CT and consultation with cardiac surgeons. The master model production process is detailed in the following sections. An example of segmented data and the corresponding finalized digital master model can be seen in fig. 2-5.

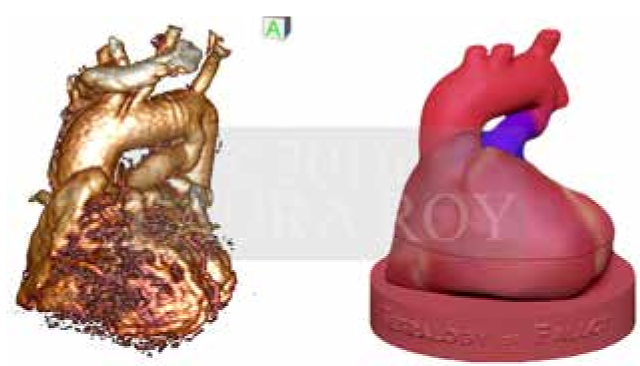

Fig. 2-5: Tetralogy of Fallot models. Left: segmented CT data. Right: final digital model

Fig. 2.6: CT slices shown from fig. 2-4 with isolated cardiovascular structures (text not intended to be read)

SEGMENTATION OF HEART SURFACES

DICOM files were imported into Purview® Horos® open source medical viewer software. The dataset was opened in the 3D Volume Renderer. The cropping tool was used to observe the cardiac area of interest while in 16-bit CLUT (“Color Look Up Table”) Mode using the high contrast 3D preset. The scissors tool was used to isolate desired cardiovascular structures. In preferences, “Use Spline for Scissors ROI” was initiated to render the scissor ROI (region of interest) as a closed Bezier spline. Cardiovascular structures were isolated by drawing an ROI spline around an area, then pressing the “delete” key to hide the pixels within the ROI, or pressing the “return” key to hide the pixels outside the area. Accidental deletions were restored by drawing around the perimeter of the area then pressing the “tab” key. The scissor state was stored within the DICOM to recall later as necessary.

After isolating the cardiac tissue with the scissor tool (fig. 2-6, fig. 2-7), the CLUT within the histogram was adjusted to maximize the pixel value for both internal and external cardiac surfaces (fig. 2-8). Pixel values for each CLUT peak were recorded.

The dataset was subsequently opened in the Horos 3D Surface Rendering viewer.

Fig. 2.7: Cardiovascular structures trimmed with scissors tool in Horos® (text not intended to be read)

Decimation and smoothing were turned off, and resolution was set to the highest value. Pixel values from the 3D Volume Render histogram were used as a guide for surface evaluation and adjusted as necessary to produce a model with minimal noise. The optimal pixel value for each volume varied by data set.

Fig. 2-8: Histogram and CLUT corresponding to fig. 2-6 (text not intended to be read)

Surface renders were generated for internal and external surfaces and exported as 3D mesh files using the Wavefront (.obj) file format.

MODEL CREATION IN ZBRUSH® 4R7

The workflow (summarized in fig. 2-9) used to produce the final models in ZBrush is described in the following sections.

Fig. 2-9: Workflow summary for transforming segmented volumes to a digital heart model

SCALE CALIBRATION AND MEASUREMENT SYSTEM

Within ZBrush, the PolyMesh 3D star was drawn onto the canvas and duplicated to accommodate importation of both heart surface .obj files. To ensure accurate measurement and scaling within ZBrush, reference units were set to mm (Preferences>Transpose Units), and export scaling (Tools>Export>Scale) was set to 1. To ensure the transpose units were consistent with ZBrush's internal measurements, the scale (Tools>Geometry>Scale) was verified against a transpose line drawn with the model in a standard view. The verified scale was then synced to all subtools simultaneously by using ZPlugins>Subtool Master and using the Scale Offset function.

Measurement of any structure was then possible by drawing a transpose line and reading the measured length at the top left of the screen. Alternately, a sphere sized to a measurement of interest (e.g. 2mm) was produced or imported. By placing the sphere at the location to be measured, thickness could be compared relatively (e.g., if a 2mm sphere protrudes from both sides of a wall's geometry, the wall is thinner than 2mm). These measurement techniques were used throughout the production process.

IMPORTING THE MESHES

The internal and external heart surface .obj files were imported into ZBrush to replace the PolyMesh 3D stars, at which point they were reclassified from .obj's to ZBrush subtools. The subtools were duplicated and one of each was reserved for reference as a high resolution, unaltered version.

REPAIRING AND SIMPLIFYING THE SURFACES

The "Auto Groups" function was applied to both internal and external surface subtools (Tool>PolyGroups>Auto Groups) to isolate non-contiguous geometry artifacts (fig. 2-10). The artifacts were hidden and deleted. Surfaces were further adjusted as necessary to repair holes and to simplify unnecessary detail and noise using the DynaMesh (Tool>Geometry>DynaMesh) process at a medium resolution (~500-750). The hi-resolution reference subtools were used to project detail (Tool>Subtool>Project) onto the lower-resolution DynaMeshed subtools. DynaMesh resolution was increased to accommodate desired detail and the projection process was repeated as necessary. The "Project" function was used in combination with the ZProject brush to maintain accurate anatomical relationships throughout the remainder of the modeling process. Other anatomical adjustment was done at this time based on references and cardiac surgeon feedback, such as removing an anomalous left superior vena cava irrelevant to the goals of the CHD model (fig. 2-11) and trimming length of the great vessels. The subtools were resized to the desired final outcome of roughly 8-10cm in each dimension.

ISOLATION OF ANATOMICAL FEATURES

As seen in fig. 2-12, the internal cardiac surface subtool was divided into polygroups corresponding to anatomical features (e.g. vena cava, right atrium, right ventricle, pulmonary trunk...) by using selection brushes to hide geometry and by redefining polygroups (Tool>Polygroups). The subtool with finalized polygroups was duplicated, and one duplicate was saved as a reference. In instances of particularly complicated anatomy, polygroups were split into separate subtools and manipulated individually (Tool>Subtool>Split) (fig. 2-13).

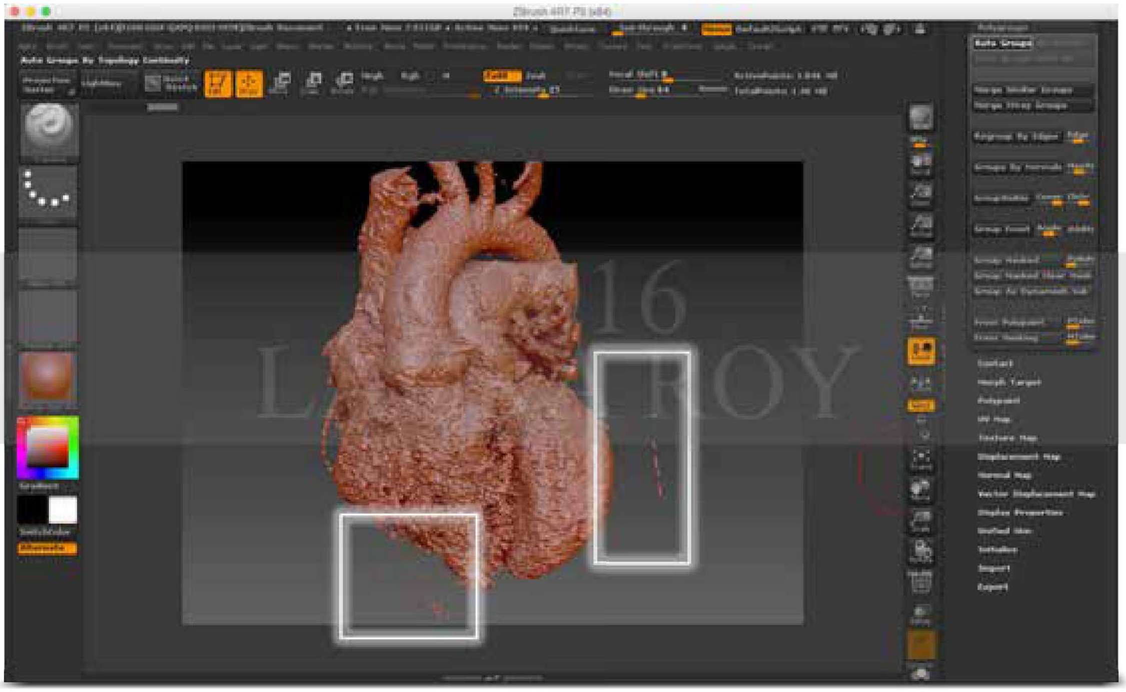

Fig. 2-10: Internal heart surface from transposition of the great arteries CHD, as imported into ZBrush. Undesired geometry artifacts are indicated within white boxes. (Text not intended to be read)

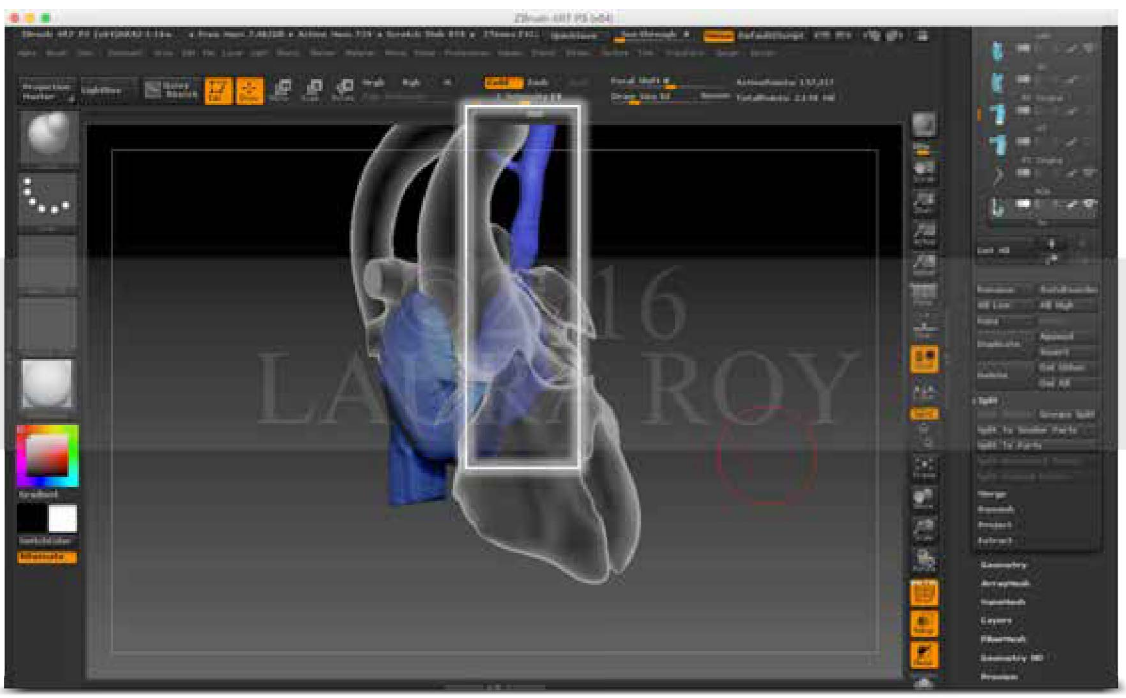

Fig. 2-11: Internal heart surface of heart with aortic root aneurysm. An anomalous left superior vena cava (in white box) draining into the right atrium was removed for teaching clarity. (Text not intended to be read)

GENERATING EXTERNAL SURFACE VESSEL WALLS

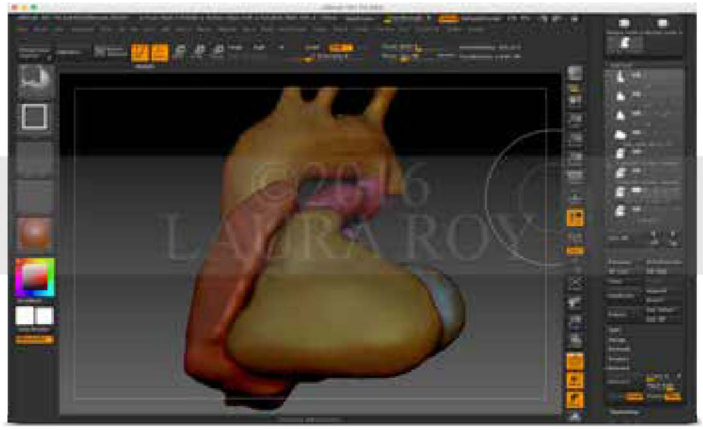

Fig. 2-12: Tetralogy of Fallot internal heart surface separated into polygroups (text not intended to be read)

Fig 2-13: Tetralogy of Fallot internal heart surface separated into subtools. The aorta (yellow) is shown in relation to other structures of the heart (semi-transparent). (Text not intended to be read)

The geometry at the points of inflow and outflow of the great vessels was hidden on the internal surface of the heart, and a subtool extraction (Tool>Subtool>Extract) was performed to produce a shell defining the myocardial-blood volume border. Thin Border ("TBorder" button) was activated within the extract settings, and other settings used were Smt 5, and Thick 0.015, although the thickness was sometimes adjusted based on the intended printing technique and the amount of scaling initially applied to the mesh. Polygroups were retained. The resulting mesh mimics the thickness of the vessel walls. The average aortic wall thickness is roughly 1mm in an infant (Skilton et al, 2005). Any thickness in this range was determined acceptable for didactic purposes. It was critical to verify that wall thickness met any requirements for an intended printing technology. Walls were measured using techniques described previously. The extracted vessel subtool was duplicated, and one duplicate was saved for reference.

ADJUSTING THE EXTERNAL SURFACE OF THE HEART

The great vessels of the external heart surface were deleted. The external heart surface was DynaMeshed to retopologize (fig. 2-14), then anatomical detailed was projected using the reserved high-resolution subtool. The resulting external heart surface subtool was further sculpted to most accurately reflect the heart's anatomy and to interact with the extracted vessel mesh.

ASSEMBLING THE COMPLETE HEART

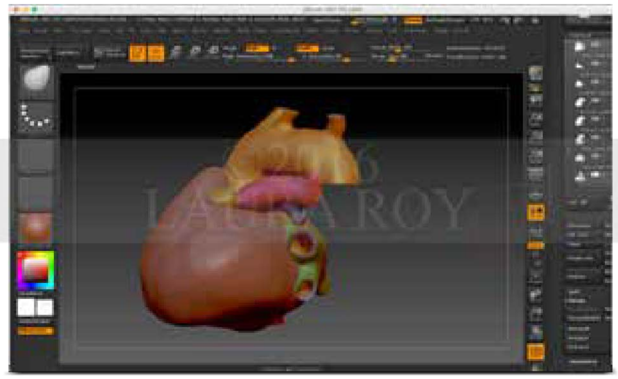

Fig. 2-14: External heart (brick-colored mesh) during the sculpting process (text not intended to be read)

The procedure for Boolean functions in ZBrush is described by Pixologic (2016). To complete a heart model, the extracted vessel subtool was merged with an external heart surface subtool using a DynaMesh Boolean addition. The internal heart surface was subtracted using a DynaMesh Boolean subtraction function. Both of these functions were performed with polygroup preservation enabled. The resulting “complete heart” was a simplified but anatomically proportionally faithful heart with preserved polygroups.

Detailed sculpting, painting, and/or remodeling of the external surface of the heart began at this stage and was adjusted as necessary through the remainder of the modeling process.

SEPARATING THE HEART INTO MULTIPLE PARTS

As determined by the didactic goals for each CHD, a complete heart was divided into parts based on a best cross-section or window. Separation of these parts was done either by selection and deletion of hidden geometry or by Boolean operations. For a straight cut, either method was used depending on convenience. For an irregular cut, the Boolean operation was used.

To separate by the selection method, the full heart subtool was duplicated, and geometry was

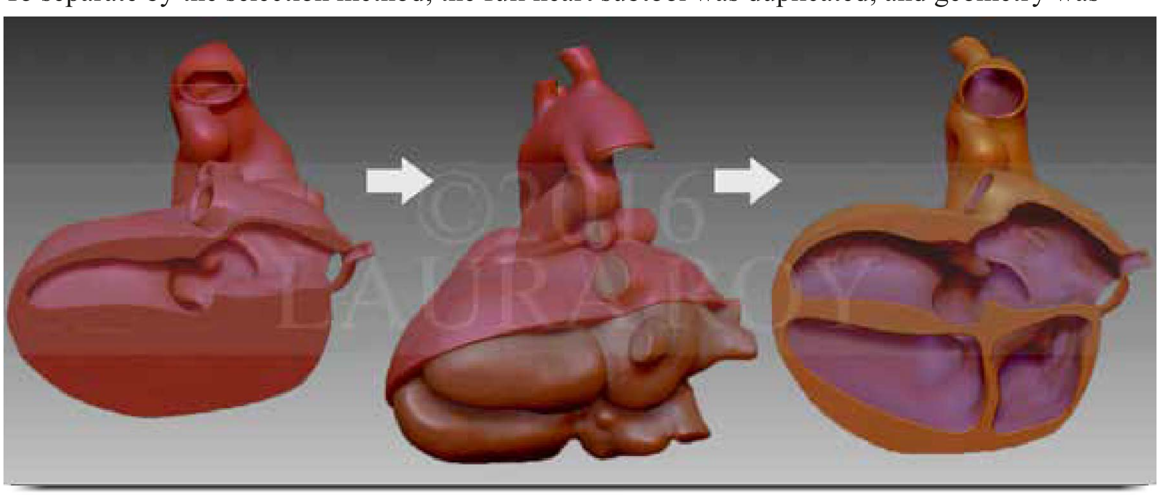

Fig. 2-15: Left: after deleting the bottom half and applying the “Close holes” function, ZBrush mistakenly closes desired holes. Middle: preparing to subtract the negative space subtool. Right: The top half of the heart after the subtraction

hidden using the selection tool. The subtool was duplicated again and the visible geometry was reversed. This resulted in two subtools with opposite visible geometry. Within the Tool>Geometry menu, “Delete hidden” and “Close holes” functions were consecutively applied to both subtools. This typically resulted in undesirable closure of some holes.

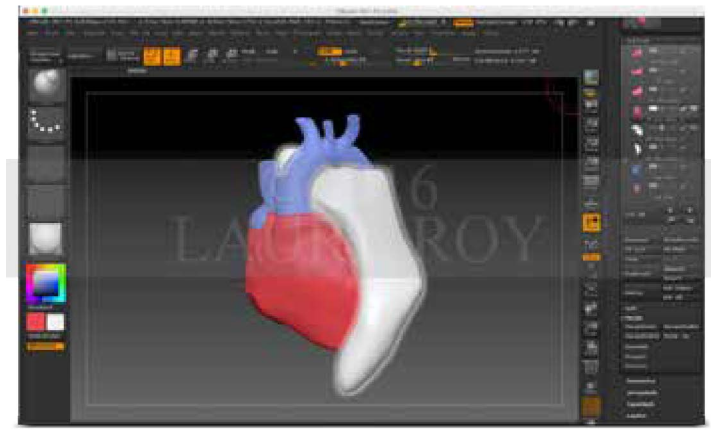

Fig. 2-16: Heart with sculpted geometry (white glowing mesh) for defining irregular boundaries when splitting the model into multiple parts (text not intended to be read)

This problem was resolved by taking the internal heart surface subtool and performing a Boolean subtraction from the complete heart half. DynaMesh was set to a high resolution (roughly 900-1200) to prevent mesh degradation of the vessel walls (fig. 2-15).

The alternate method of splitting a heart was similar, except that instead of initially separating the heart by deleting a hidden selection, an appended subtool served as a Boolean operator. As seen in fig. 2-16, a white mesh is covering the left half of a heart. By taking a Boolean subtraction of the mesh and a Boolean intersection of an identical mesh, irregular interlocking halves were created.

REGISTRATION

Registration points were created by DynaMeshing two wide capsule-shaped subtools to add volume to the inferior half of a model and to subtract volume from the superior half. This resulted in interlocking geometry between multiple parts to prevent slippage and to ensure proper alignment of parts (fig. 2-17).

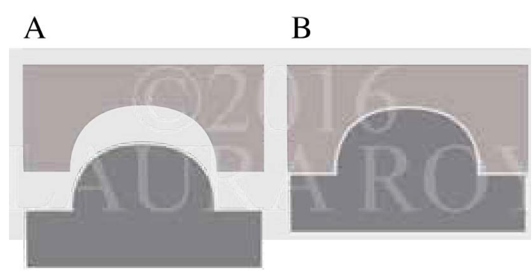

Fig. 2-17: Registration. A: Multiple parts of a model. B: model parts held together with interlocking geometry

PRODUCING A CUSTOM BASE

A supporting base was built by Boolean subtraction of the heart model in anatomical position from a cylinder. Text was applied to the cylinder by using the inflate brush with a text alpha and focal shift at the widest setting of -100.

3D PRINTING OF MODELS

The process for further preparing the model for 3D printing was largely determined by the anticipated printer technology. It is summarized in fig. 2-18 and detailed as follows.

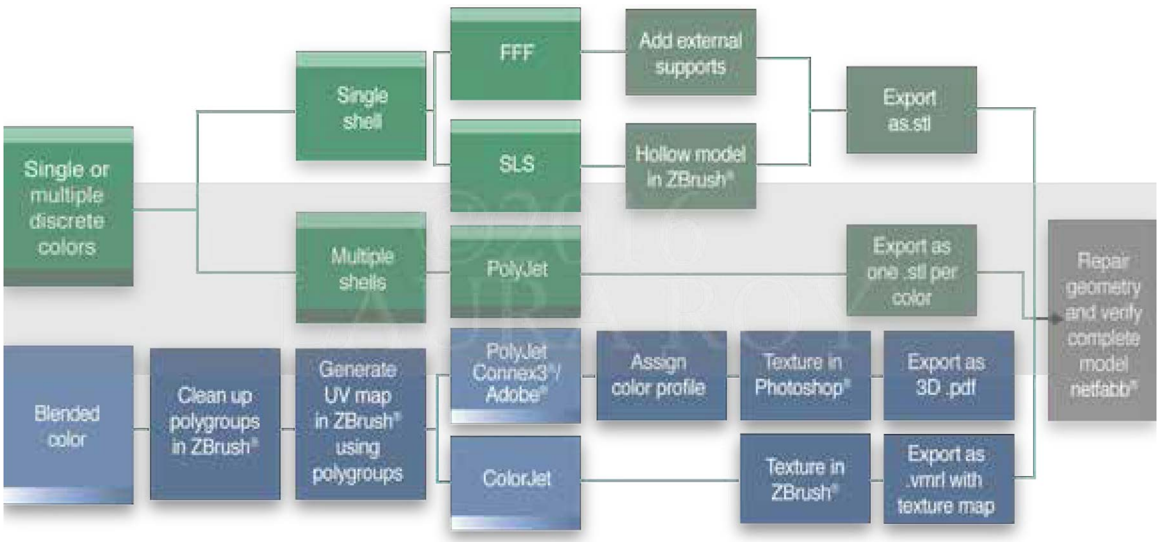

Fig. 2-18: Workflow summary for preparing models for 3D printing in various materials

SINGLE COLOR PRINTING

Within the scope of this project, 3D prints using only one color of material were producing using Fused Filament Fabrication (FFF) and Selective Laser Sintering (SLS). For FFF, no additional alteration to the model was required for production because of printing software ability to optimize printing. However, it was necessary to generate support geometry for overhangs, and this was done in either AutoDesk® MeshMixer® or Ultimaker® Cura.® For SLS, no supports were needed but models were designed with thin walls and hollowed when possible to reduce material cost.

FFF concept models were produced using the Printrbot® Simple Metal 3D printer using PLA filaments. The build plate was lined with painter's masking tape, then treated with alcohol. Models were prepared for printing using MeshMixer to orient the model to the printer build plate.

Columnar post supports were generated as needed within MeshMixer. The default setting of posts with 3mm diameter was supplemented with additional supports with diameters of 4-5mm added manually (fig. 2.19). Some FFF models were also outsourced to 3Dhubs.com and printed in red ABS.

The model was exported from MeshMixer and loaded into Cura. New or additional supports were generated in Cura as needed using the brim and line support settings, and printing settings were adjusted. For PLA, the layer height was adjusted to 0.1mm, and the printing temperature (C) was adjusted to 200.

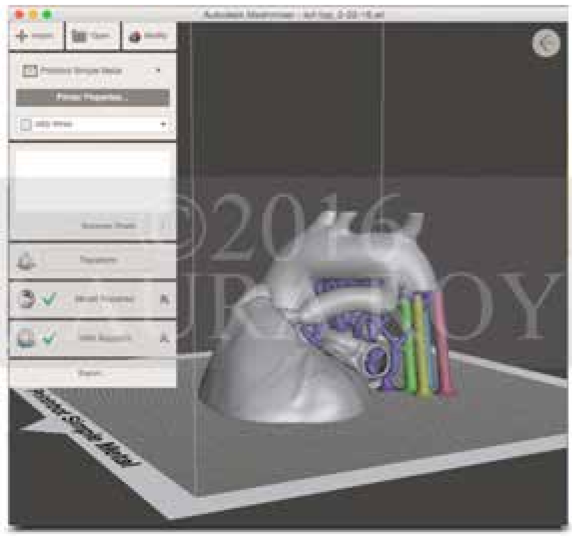

Fig. 2-19: Model (grey) in MeshMixer® with automatically generated supports (purple). Manually added supports are shown in pink, yellow, and green. (Text not intended to be read)

Printing (fig. 2-20) was observed closely during the first 5-10 layers of filament application to ensure even application. Wire cutters were used to remove undesirable material buildup. After printing, supports were removed manually. Models were left as is or were airbrushed with acrylic paint to test color combinations and didactic approaches.

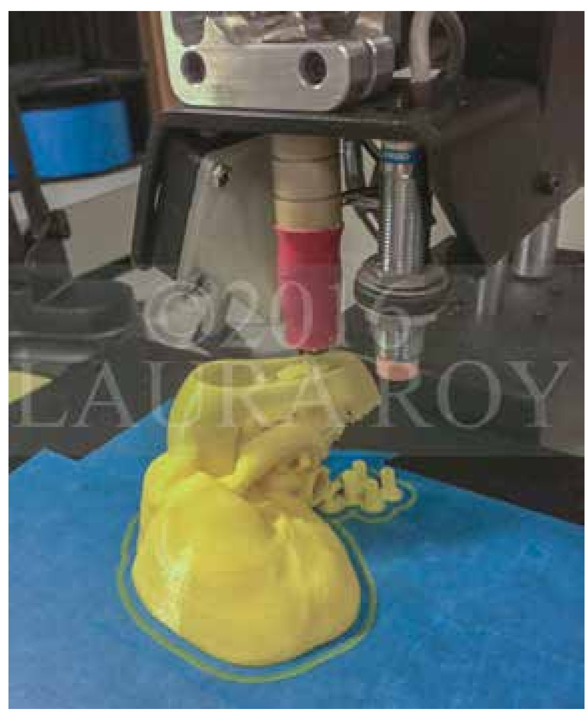

Fig. 2-20: FFF Printing in progress. The extruder head (red) deposits layers of yellow PLA to build up the model

For SLS, cost was determined by material volume and machine space volume. To minimize cost, models were created with thin walls and/or were hollowed. Hollowing a model required adding one or more vent holes so unsintered powder could be removed after printing was completed. Depending on the size of the print, multiple holes or a larger hole was required.

Models were hollowed using ZBrush's

DynaMesh Create Shell operation. A location was selected for the vent hole(s), and a circular mask was drawn. The mask was extracted (Subtool >Extract) to form a cylinder. The cylinder was set as a Boolean subtraction object in the subtool properties. It was merged together with the model to be hollowed (Tool>Subtool>Merge>Merge Down). A shell (fig. 2-21) was created (Tool>DynaMesh>Create Shell), with the "Project" setting turned off. Shell thickness was determined by the size of the DynaMesh unit, e.g., a shell thickness of 4 will produce walls that are four DynaMesh polygons in length. The DynaMesh resolution was set sufficiently high to prevent mesh degradation, usually about ~1000. SLS printing was outsourced to Shapeways, Inc.

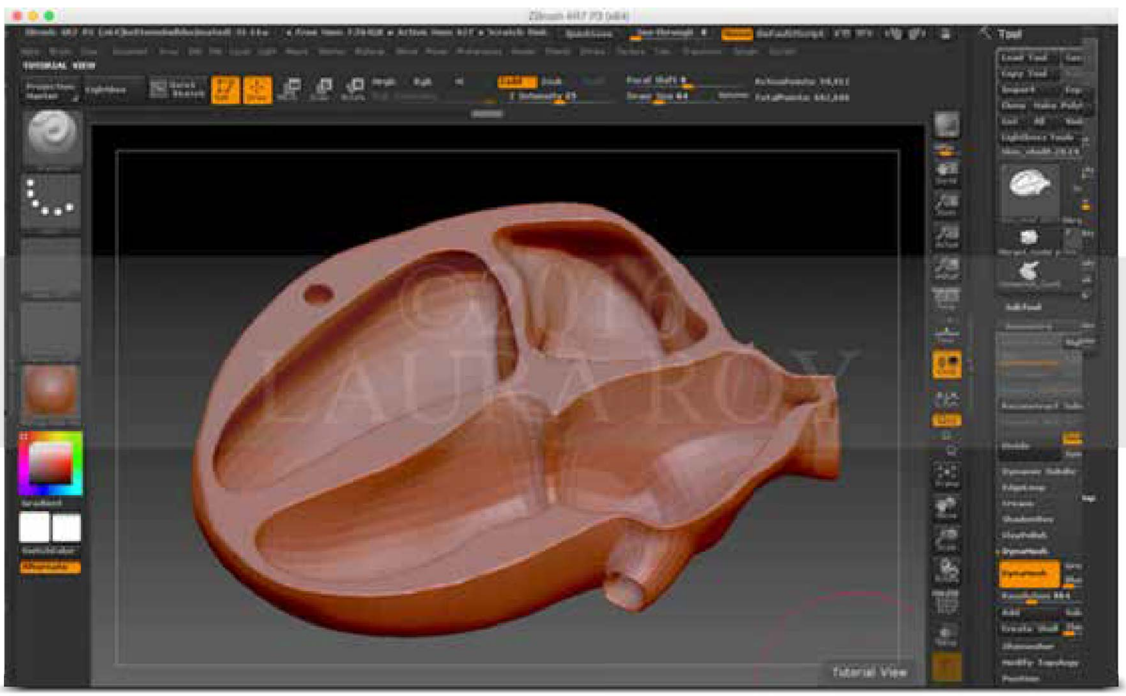

Fig. 2-21: Hollowed model with vent hole (text not intended to be read)

MULTI-SHELL POLYJET PRINTING

PolyJet printing in its traditional format allows for one material to be printed per closed geometry mesh, or "shell." Multiple non-overlapping shells can coexist in a single model, and each model can hence contain many materials or material blends. However, a single shell cannot have more than one material or material blend. To produce a model with discrete shells, three techniques were used: extraction by masking, extraction from polygroups, and a Boolean technique.

For shells created by masking (fig. 2-22), an area was masked either with a freehand brush or, in the case of detailed geometry like numbers, masks were applied using an alpha mask with the brush focal shift at its widest setting (-100). The "Extract" operation (Tool>Subtool>Extract) was used to produce new geometry in the shape of the mask. Best results occurred when the model was subdivided prior to extraction.

Fig. 2-22: Multi-shell object. Yellow numbers on the model are separate shells produced by extracting masked areas. Blue areas were produced with the Boolean technique.

By using polygroups retained throughout the modeling process, geometry was also extracted to correspond with individual anatomical structures. Prior to extraction, edge loops were created around polygroups to ensure smoother resulting geometry (Tool>Geometry>EdgeLoop>GroupsLoop). New loops were merged with existing adjacent polygroups. Additional polygroups were created for additional shell extractions using the selection or slice brushes (fig. 2-23, fig. 2-24).

To produce multiple shells when adding volume to the model through extraction was undesirable, the Boolean technique was used. A sphere subtool ("Boole geometry") was

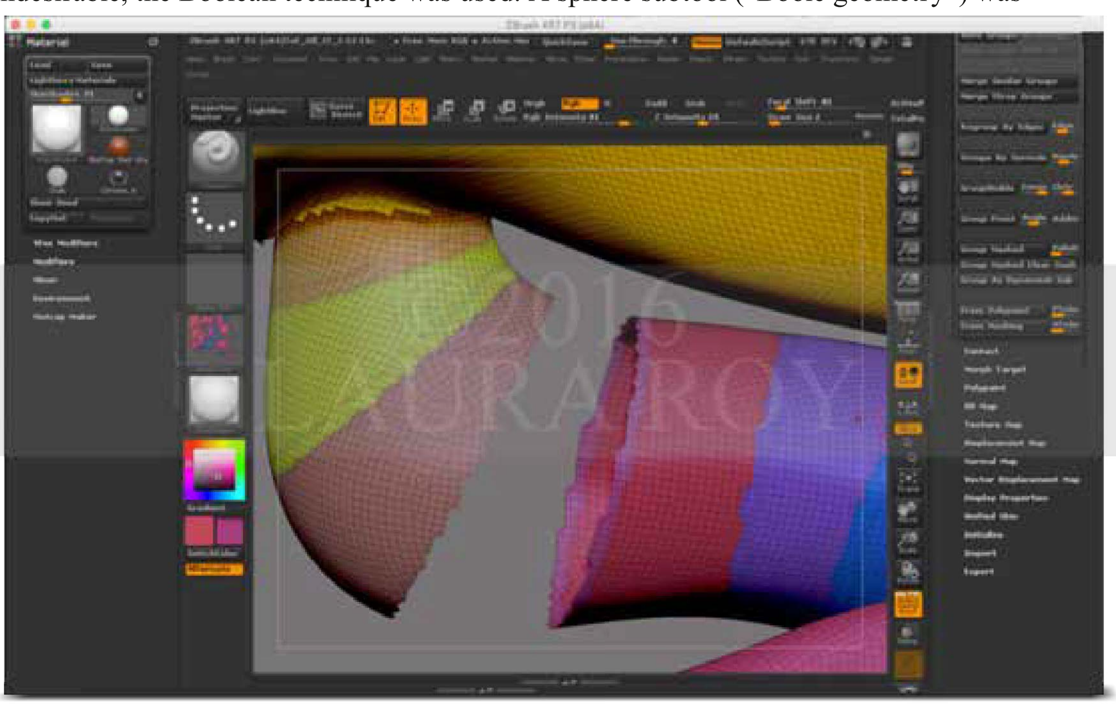
Fig. 2-23: Additional polygroups for multiple extracted geometries (Text not intended to be read.)

appended. The Boole geometry was manipulated to intersect the model where the new shell was wanted. The model and the Boole geometry were duplicated. A subtraction Boolean operation was performed on one pair (model and Boole geometry), and an intersection Boolean operation was performed on the other pair to yield interlocking shells (blue structures in fig. 2-22).

BLENDED COLOR PRINTING

ColorJet and PolyJet were both used to produce blended color 3D prints. ColorJet was used to print CMYK color on a white/light colored sandstone base material, and PolyJet used Connex3/ Adobe technology to print with a restricted, three-color palette. Both methods required a texture file in addition to a polygonal model with a UV map (to map color in a 2D file to the 3D object).

The UV Map was produced to accompany each model for blended color printing in ZBrush. Existing polygroups in a model were used as the basis for the UV map. Edge loops were generated based on polygroups and individually merged into adjacent polygroups to produce clearly defined borders.

Fig. 2-24: Tetralogy of Fallot for PolyJet printing with shells produced by polygroup extraction. Left: superior. Right: inferior.

Under the (ZPlugin>UV Master), the symmetry setting was deactivated and the polygroups setting was activated, then the UVs were unwrapped. A corresponding texture was created from PolyPaint (Tool>Texture Map>Create>New from PolyPaint). The texture map was exported for additional painting in Photoshop. See fig. 2-25 for a UV map and the resulting ColorJet 3D print.

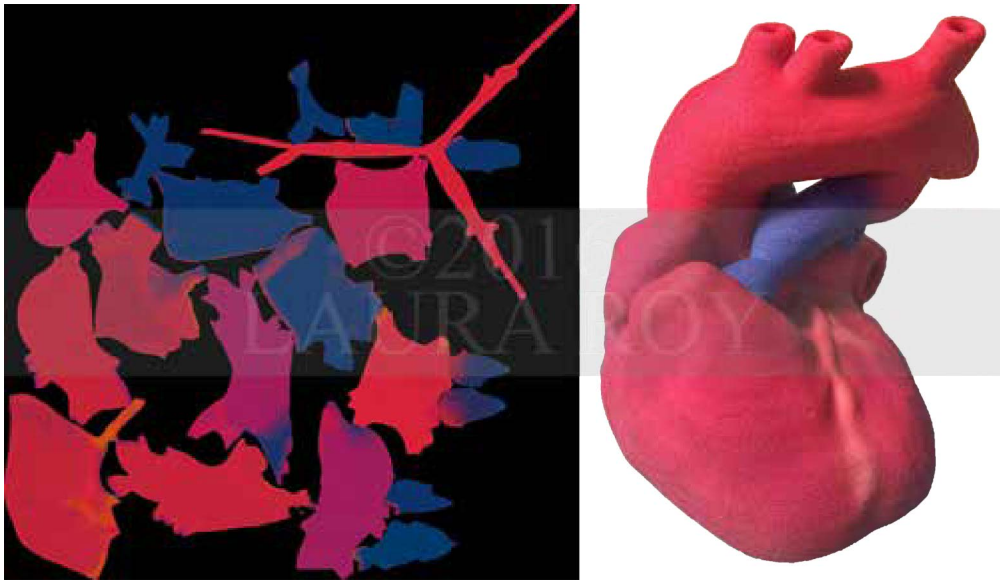

Fig. 2.25: Left: UV Map. Right: corresponding ColorJet 3D print

To print in full color, ColorJet technology was used. The model was exported for 3D printing from ZBrush as a .vmrl file (ZPlugin>3D Exporter). The resulting polygonal model and texture were transferred to Shapeways, Inc. for printing.

The sandstone material of the ColorJet 3D print required post-printing treatment to decrease fragility and to prevent dirt accumulation. Smooth-On brand XTC-3D Brush-On Coating for 3D Printed Parts (an epoxy resin) was used to coat each 3D printed model in two passes: once for the interior surfaces and once for the exterior surfaces (fig. 2-26). Undesirable cured drips of resin were shaved off with a scalpel, leading in some cases to

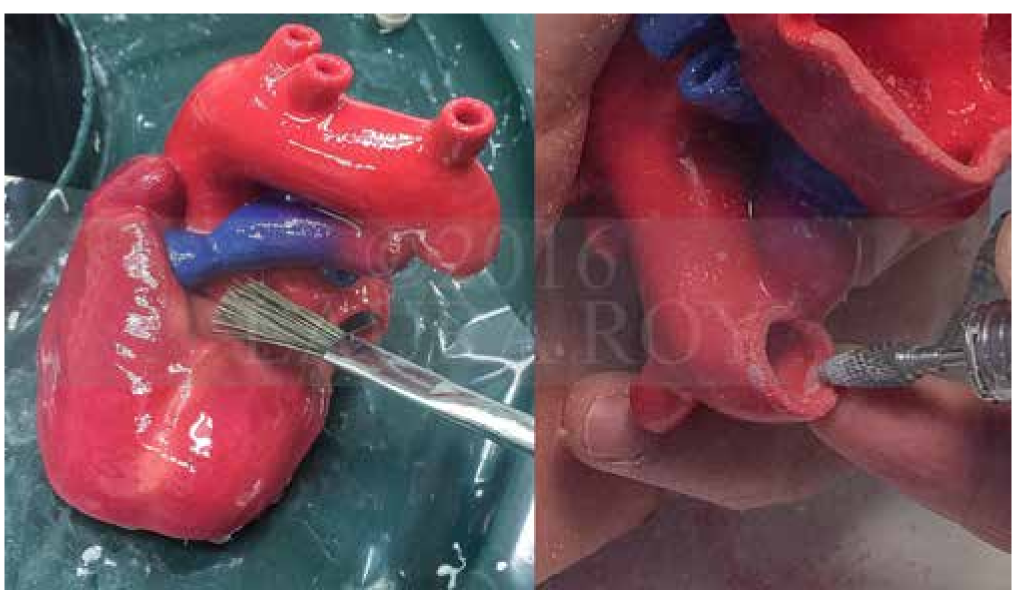

Fig. 2-26: Post-processing of ColorJet model. Left: resin treatment. Right: polishing.

delamination of the cured epoxy resin. The delaminated surfaces were ground and successfully re-treated with an additional coat of epoxy resin. The cross-section surface of the 3D print was left untreated to emphasize the cross-section.

For blended color PolyJet prints, Adobe Photoshop and Adobe Creative Color software for the Objet Connex3 printers were used. Two methods were tested for working within Adobe Photoshop to prepare files for printing with PolyJet technology. For both methods, it was necessary to preload color and printer profiles corresponding to the Stratasys Connex3 printer, which were downloaded from the Stratasys website.

In the first method, a model was imported into Photoshop. The desired PolyJet color profile (e.g., “Stratasys-CMY-Cyan843-Magenta851-Yellow836-Connex3” for CMY) was assigned. Within the 3D Properties panel for the “Scene” containing the model, Surface style was set to “Unlit Texture” to remove all shadow and ambient occlusion. To view the texture map in a new window for more detailing editing, it was opened by navigating to the model material’s diffuse map and selecting “Edit Texture.” Window arrangement was set to “2-up vertical” to show the texture map and model simultaneously. The model was painted using standard Photoshop technique (fig. 2.27). The model was painted per typical Photoshop techniques.

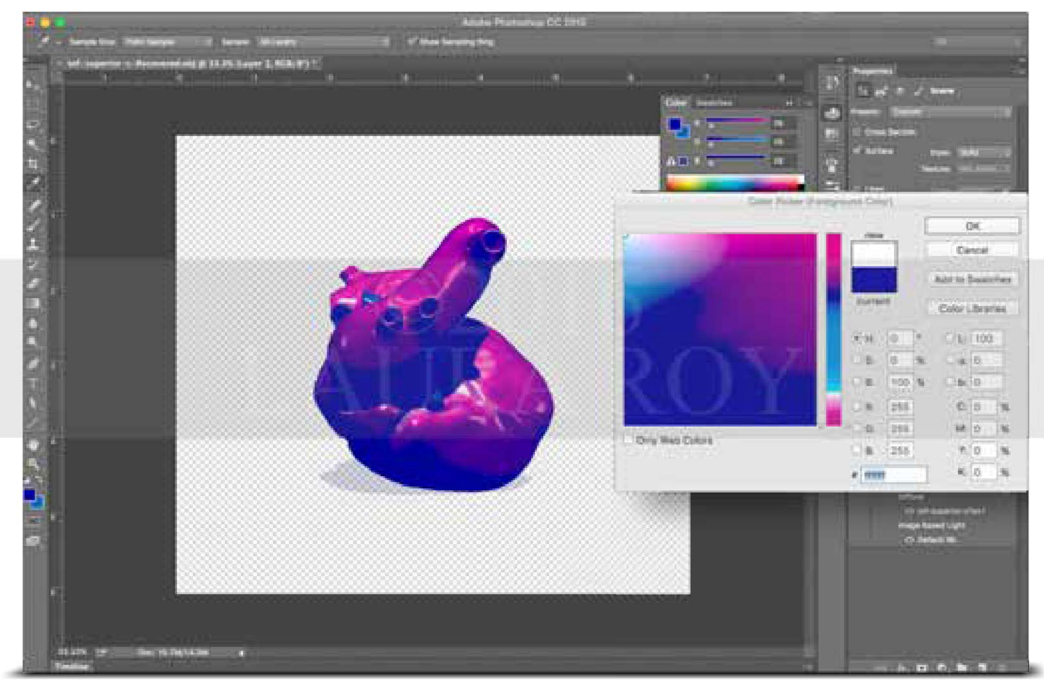

Fig. 2-27: Painting a model within Photoshop with Stratasys® white-cyan-magenta color profile (text not intended to be read)

For the second method, the model was opened in both Photoshop and ZBrush. The desired PolyJet color profile (e.g., “Stratasys-CMY-Cyan843-Magenta851-Yellow836-Connex3” for CMY) was assigned to the file in Photoshop as just described. Color was tested on the model and RGB values of desired colors were recorded. Using the RGB values as an approximate guide, the same model was PolyPainted within ZBrush. A texture map was generated in ZBrush from the PolyPaint (Tool>Texture Map>Create>New from PolyPaint). The texture map was exported from ZBrush and imported to replace the Photoshop diffuse texture map. Additional adjustments were made in Photoshop.

When painting was complete with either method, the model was prepared for printing. In the 3D Print Settings Properties menu, the “Print To” field was set to “Stratasys Direct Manufacturing,” and the “Printer” field was set to “Detailed Plastic PolyJet 3-color.” Detail was left at high and the scale volume was verified and adjusted if necessary. Then, the “Start Print” button was pressed to generate a 3D PDF and estimate (fig 2-28). The files were uploaded to Stratasys Direct Manufacturing, who provided an additional 3D PDF proof and estimate. Models were printed on an Object 500 Connex3 printer (fig. 2-29, fig. 2-30).

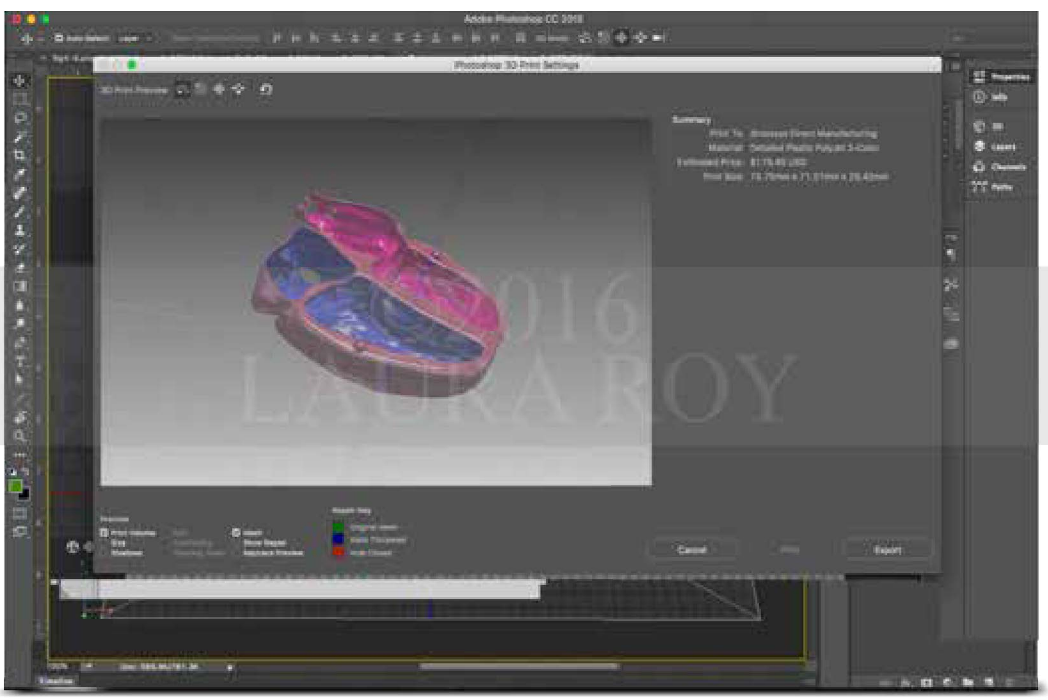

Fig. 2-28: 3D PDF preview of a model in Photoshop (text not intended to be read)

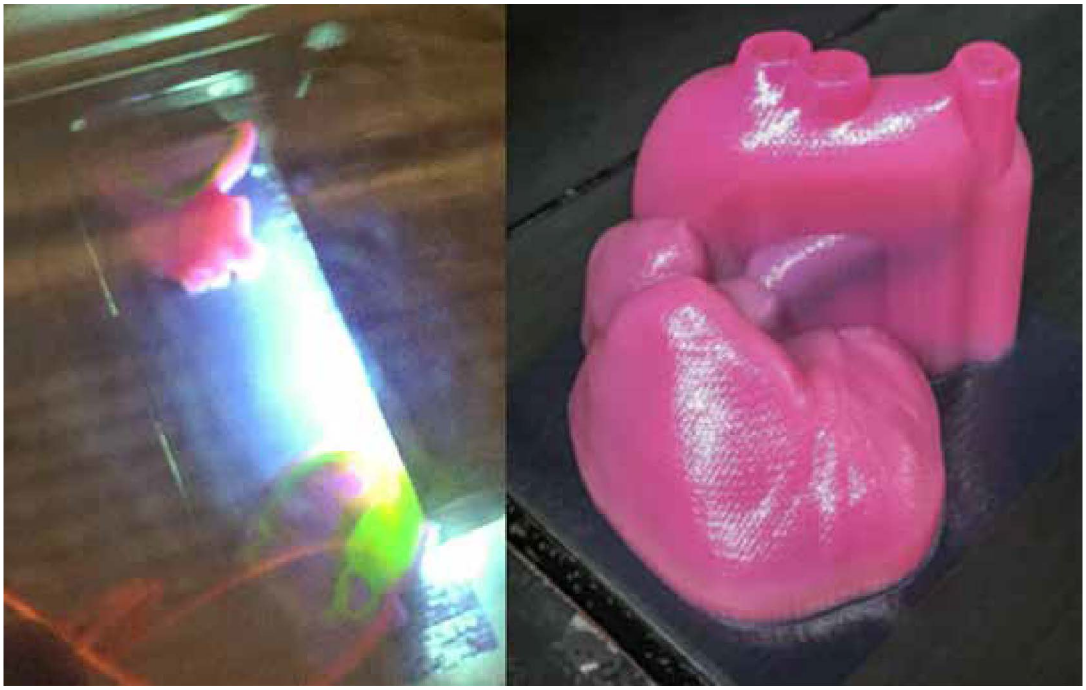

Fig. 2-29: Production of Tetralogy of Fallot model in PolyJet using cyan, magenta, and yellow. Left: printing in Connex3; right: printed model prior to rinsing support material. Credit for photos: CJ Stein (used with permission).

Fig. 2-30: Polyjet model. Left: after support material was removed. Right: model in Connex3 3D printer.

Following printing, support material was removed from the PolyJet prints using a high pressure water jet. One model was coated with a clear coat of high gloss urethane to produce a shiny, smooth surface versus the untreated matte surface.

FINAL OPTIMIZATION OF MODELS FOR GENERAL 3D PRINTING

Models to be used for 3D printing had to be watertight (the model could not have any holes), and manifold (the model could not have overlapping geometry or incongruent normals). Models were analyzed in the software netfabb Basic to ensure clean geometry and repair any problems as necessary using the default simple repair setting (fig. 2-31).

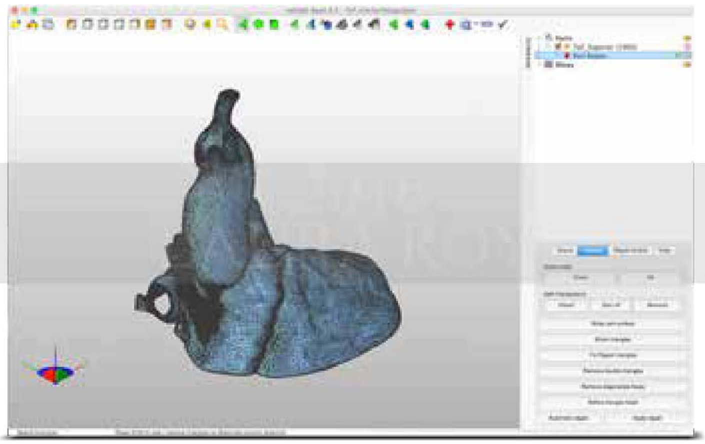

Fig. 2-31: Digital model in netFabb Basic® to repair 3D printing issues (text not intended to be read)

The models for 3D printing were also checked for walls thickness. Wall thickness specifications were referenced on per-printer basis. Walls were measured and if a wall was found to be too thin, the model was inflated in ZBrush (Tool>Deformation>Inflate) either as a whole or selectively using masking.

For extensively subdivided models (1 million or more polygons), the polygon count was decreased prior to printing. A duplicate model was created to preserve the high-poly version for reference Using the ZPlugin "Decimation Master," a subtool was pre-processed ("Pre-Process Current"). Next, "% of Decimation" was set to 5, and "Decimate Current" was applied to reduce polygons to 5% (e.g. ~500K polygons were reduced to 25K polygons). If too much detail was lost, the modification was undone and the % of decimation was set to 10 and repeated. Decimation master settings were adjusted to preserve polygroups (which could be used to rebuild a UV map), and/or PolyPaint as necessary.

CONCEPT DEVELOPMENT FOR INTERACTIVE APP PROTOTYPE

To accompany the 3D prints, supporting digital assets were also considered. Using the name "A Heart in the Hand," a logo (fig. 2-32) was designed in Adobe Illustrator®. Based on feedback from cardiac surgeons, a flowchart was produced to outline a potential web application to provide additional context to the 3D printed models.

Fig. 2-32: Logo concept

Digital models were adjusted in ZBrush for use as interactive prototypes. ZRemesher was used to retopologize meshes and decrease polygon count. Polygroups were preserved and used to rebuild UV maps.

Fig. 2-33: Testing lighting schemes in SketchFab® (text not intended to be read)

Digital models with textures were uploaded to SketchFab for use as interactive, rotatable models. Within SketchFab's 3D settings editing panel, adjustments were made on a per-CHD basis to optimize visibility. Lighting was adjusted so that models were evenly lit with two directional spot lights and one hemispherical light in addition to lighting from an environment unseen by the camera (fig. 2-33). The environment was selected to minimize color influence on the model. Annotations were added on a per model basis to indicate important anatomy. Headlines and further descriptions were written as needed (fig. 2-34). Animation was also investigated within SketchFab. Models split into sections were animated opening and closing so users could easily interact with and view both halves of the model, as well as see their relationship to each other. The animation was produced in Cinema4D. Within SketchFab, the animation could be paused for

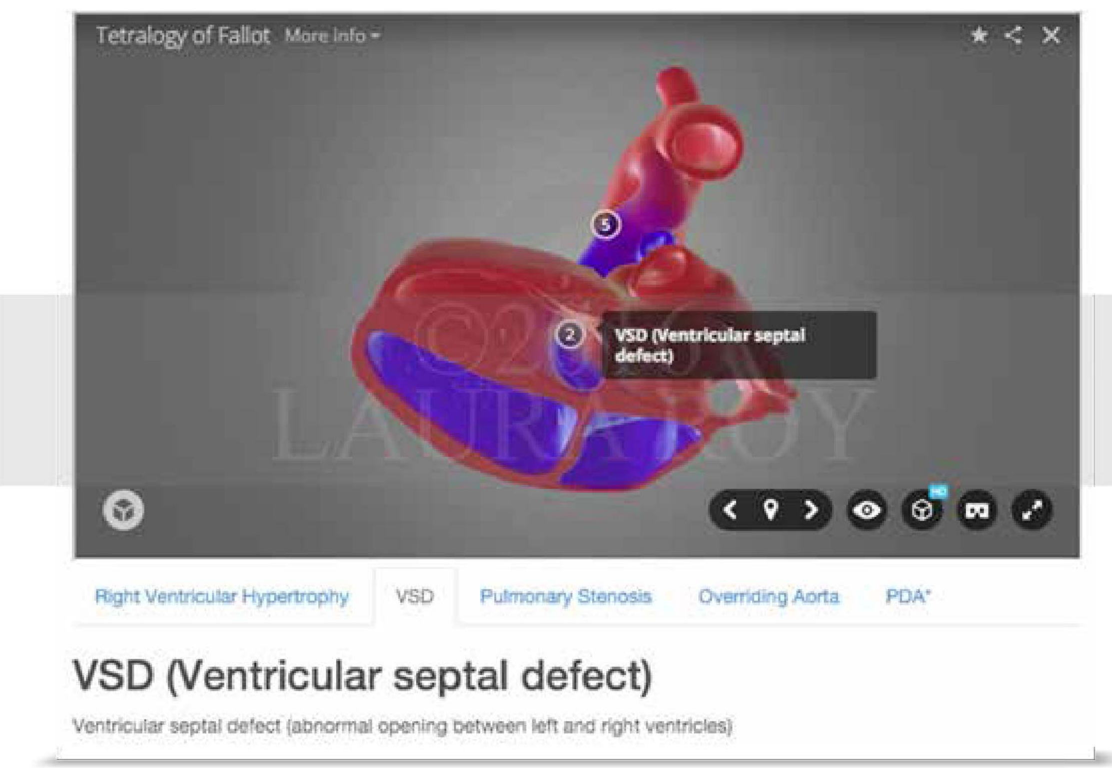

Fig. 2-34: Tetralogy of Fallot model in SketchFab with annotations and additional description (annotation box: "VSD (Ventricular septal defect)"; other text not intended to be read)

additional interactivity. Animations were keyframed to move slowly, taking between 30 seconds to 60 seconds for an opening-closing cycle, to give viewers adequate time to view models moving models (fig. 2-35). The SketchFab models were viewable in virtual reality using Google Cardboard (fig. 2-36).

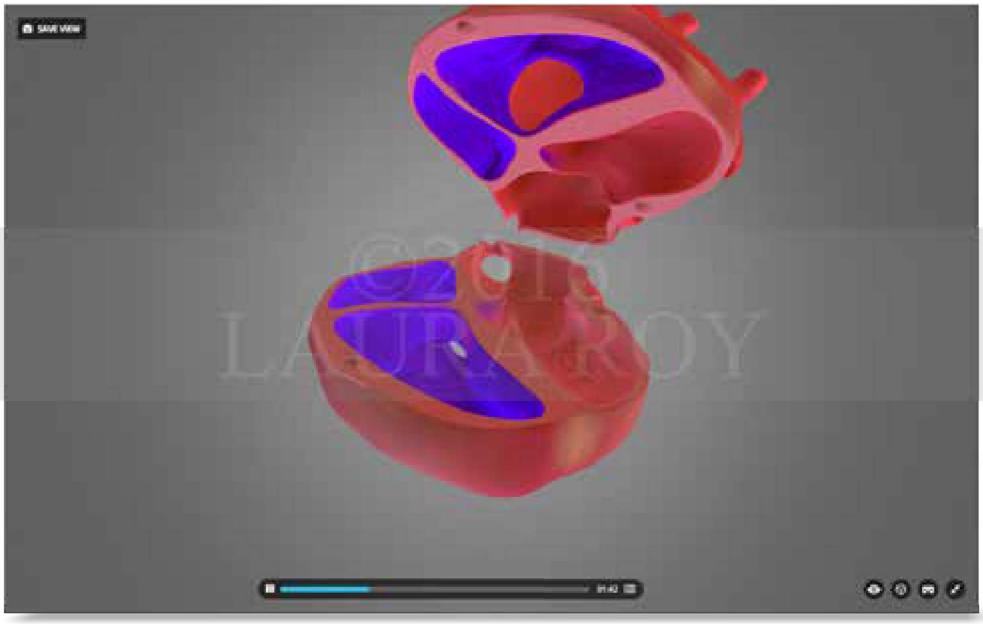

Fig. 2-35: Animated model halves

Fig. 2-36: User interacting with Google Cardboard® virtual reality digital heart model in SketchFab

RESULTS

The primary result of this research is a novel workflow for production of 3D printed models optimized for teaching a lay audience—specifically parents and families of patients with CHDs. The workflow combines didactic needs assessment, segmentation, digital modeling, and 3D printing. It integrates sub-workflows for diverse printing results. It also proposes a way to integrate production of supporting digital assets into the process.

As part of the research to determine a workflow, the following digital and tangible assets were produced:

TANGIBLE ASSETS

- 3D prints of tetralogy of Fallot CHD
    - Full color ColorJet print in sandstone material with epoxy resin treatment (fig. 3-1)
    - FFF print in yellow PLA at 0.1mm layer thickness (fig. 3-2)
    - Multi-shell color PolyJet print in flexible material blends (VeroMagenta-VeroCyan-TangoClear palette) (fig. 3-3)
    - Blended color PolyJet print (VeroCyan-VeroMagenta-VeroYellow palette) (fig. 3-4)
    - Blended color PolyJet print (Pure VeroWhite-VeroCyan-VeroMagenta palette) (fig. 3-5)
- 3D printed bespoke base for tetralogy of Fallot CHD 3D print. SLS print in white strong and flexible plastic (fig. 3-6)
- 3D prints of transposition of the great arteries CHD
    - Pre-operative anatomy: red ABS FFF print at 0.25mm layer thickness, with acrylic spot color (fig. 3-7)
    - Post-operative (Mustard procedure) anatomy: red ABS FFF print at 0.25mm layer thickness, with acrylic spot color (fig. 3-8)

DIGITAL ASSETS

- Segmented cardiac surfaces of 10 CHDs (fig. 3-9)
- Digital models of hearts with CHDs
  - Pre-operative tetralogy of Fallot (fig. 3-10)
  - Pre-operative aortic root aneurysm (fig. 3-11)
  - Post-operative aortic root aneurysm (fig. 3-12)
  - Pre-operative transposition of the great arteries (fig. 3-13)
  - Post-operative (Mustard procedure) transposition of the great arteries (fig. 3-14)
- Interactive, annotated hearts with CHDs in SketchFab
  - Pre-operative tetralogy of Fallot (fig. 3-15)
  - Pre-operative transposition of the great arteries (fig. 3-16)
- Content flowchart for corresponding app (fig. 3-17)

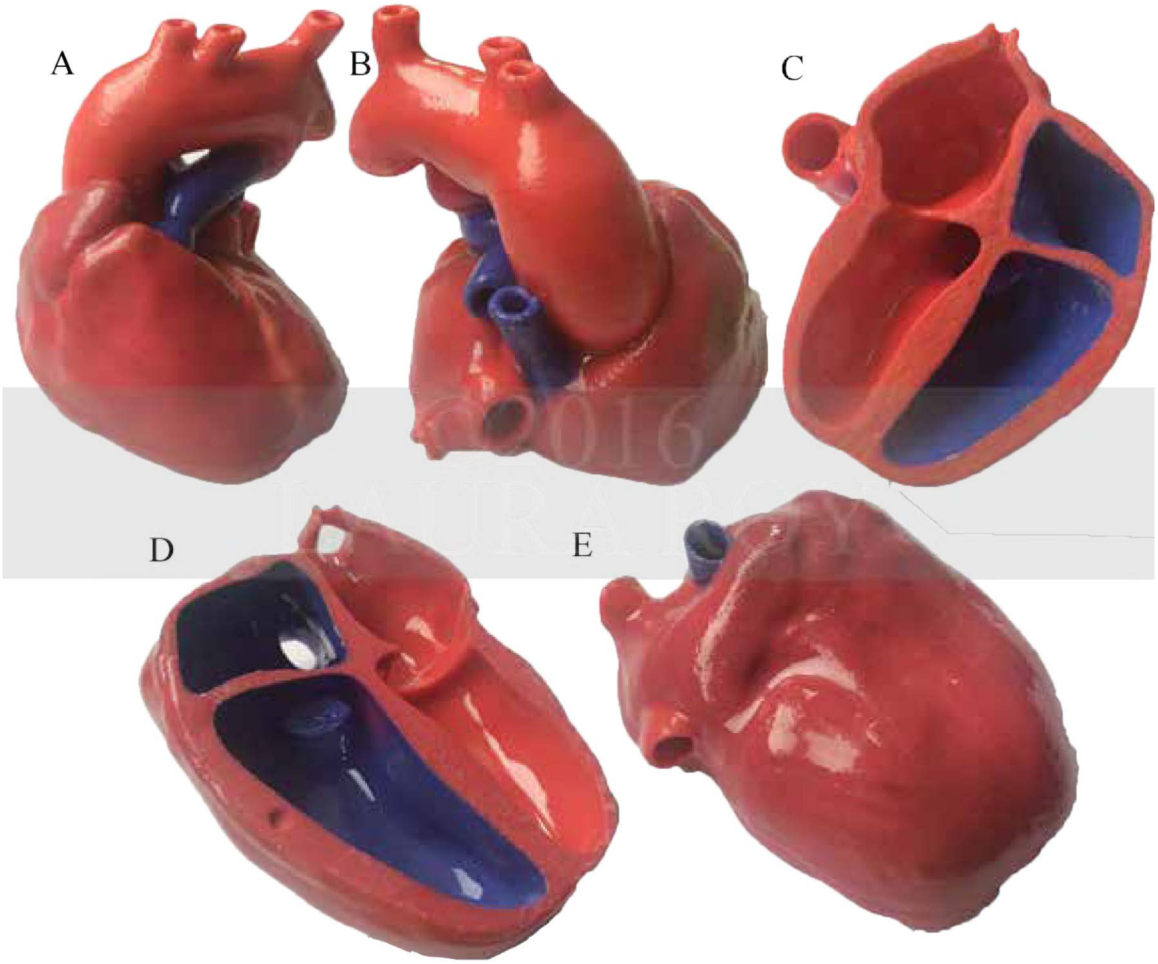

Fig. 3-1: 3D print: Tetralogy of Fallot CHD. ColorJet with epoxy resin treatment. A: superior from left anterior. B: superior from right posterior. C: superior cross-section. D: inferior cross-section. E: inferior from left posterior.

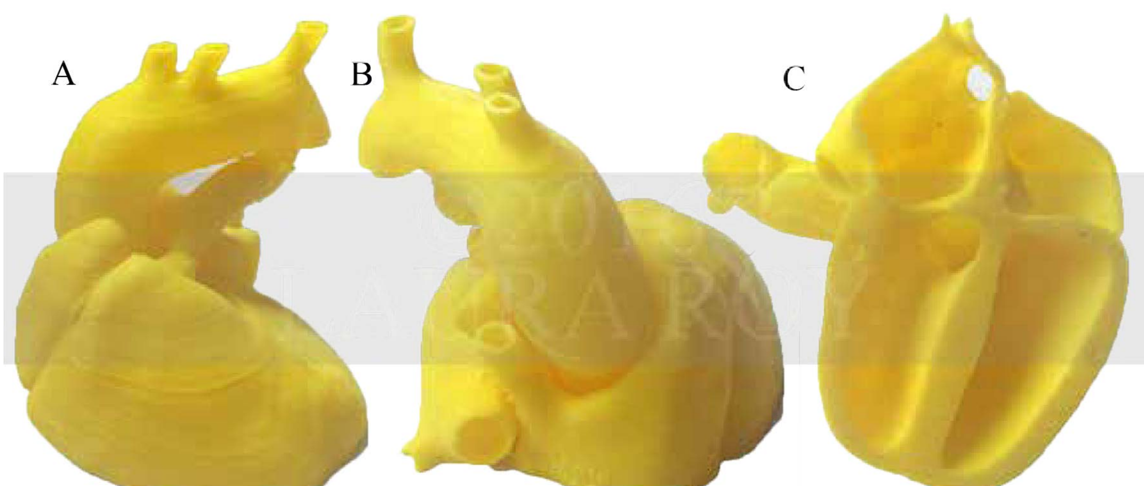

Fig. 3-2: 3D print: Tetralogy of Fallot CHD. Single color FFF print in yellow PLA. A: superior from left anterior. B: superior from right posterior. C: superior cross-section.

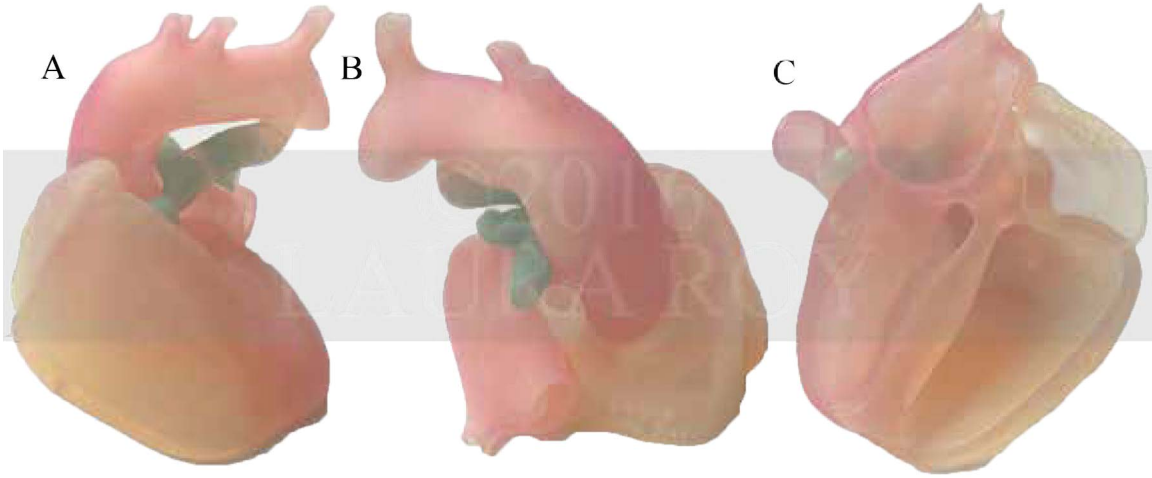

Fig. 3-3: 3D print: Tetralogy of Fallot CHD. Multi-shell PolyJet print in flexible materials using magenta-cyan-TangoClear color palette . A: superior from left anterior. B: superior from right posterior. C: superior cross-section.

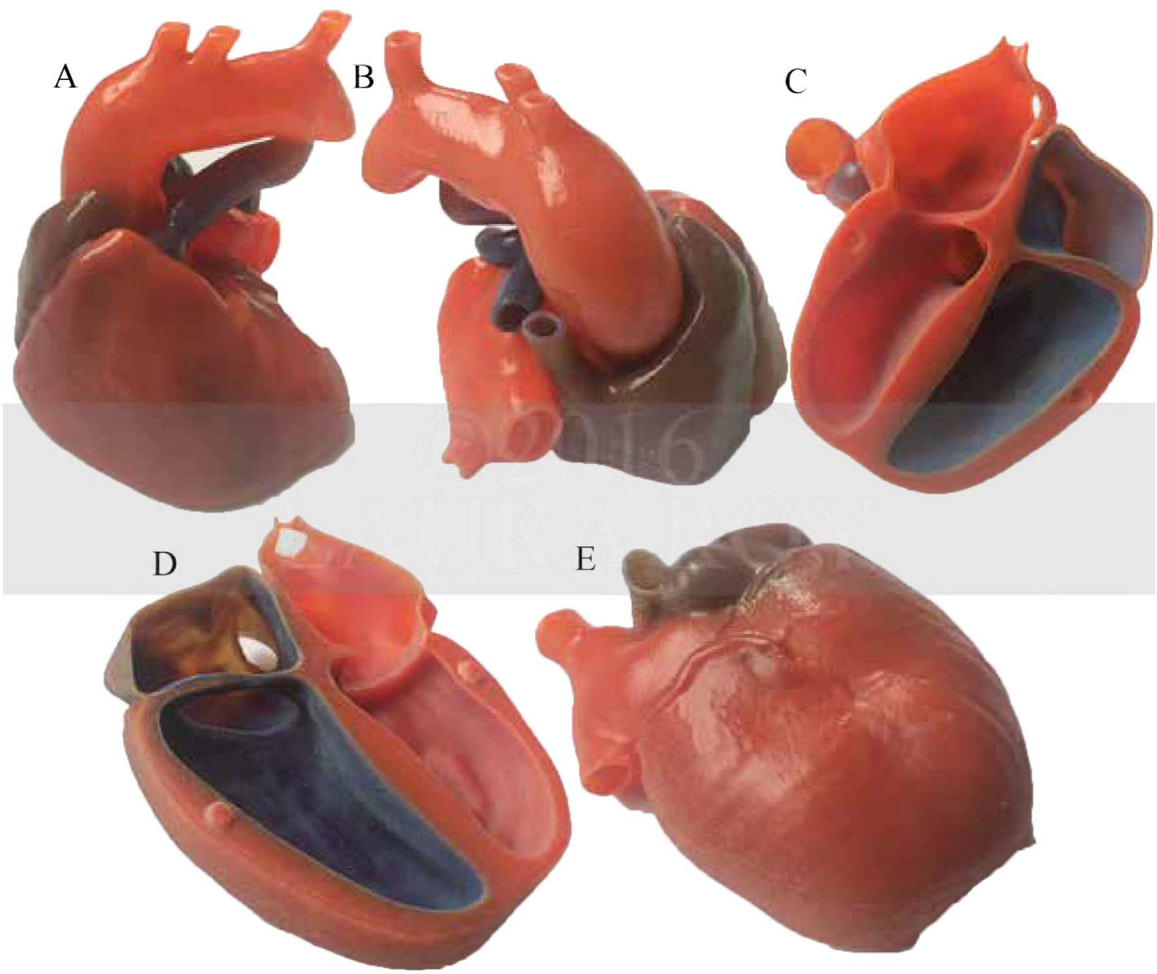

Fig. 3-4: 3D print: Tetralogy of Fallot CHD. Blended color PolyJet print in cyan-magenta-yellow color palette. A: superior from left anterior. B: superior from right posterior. C: superior cross-section. D: inferior cross-section. E: inferior from left posterior.

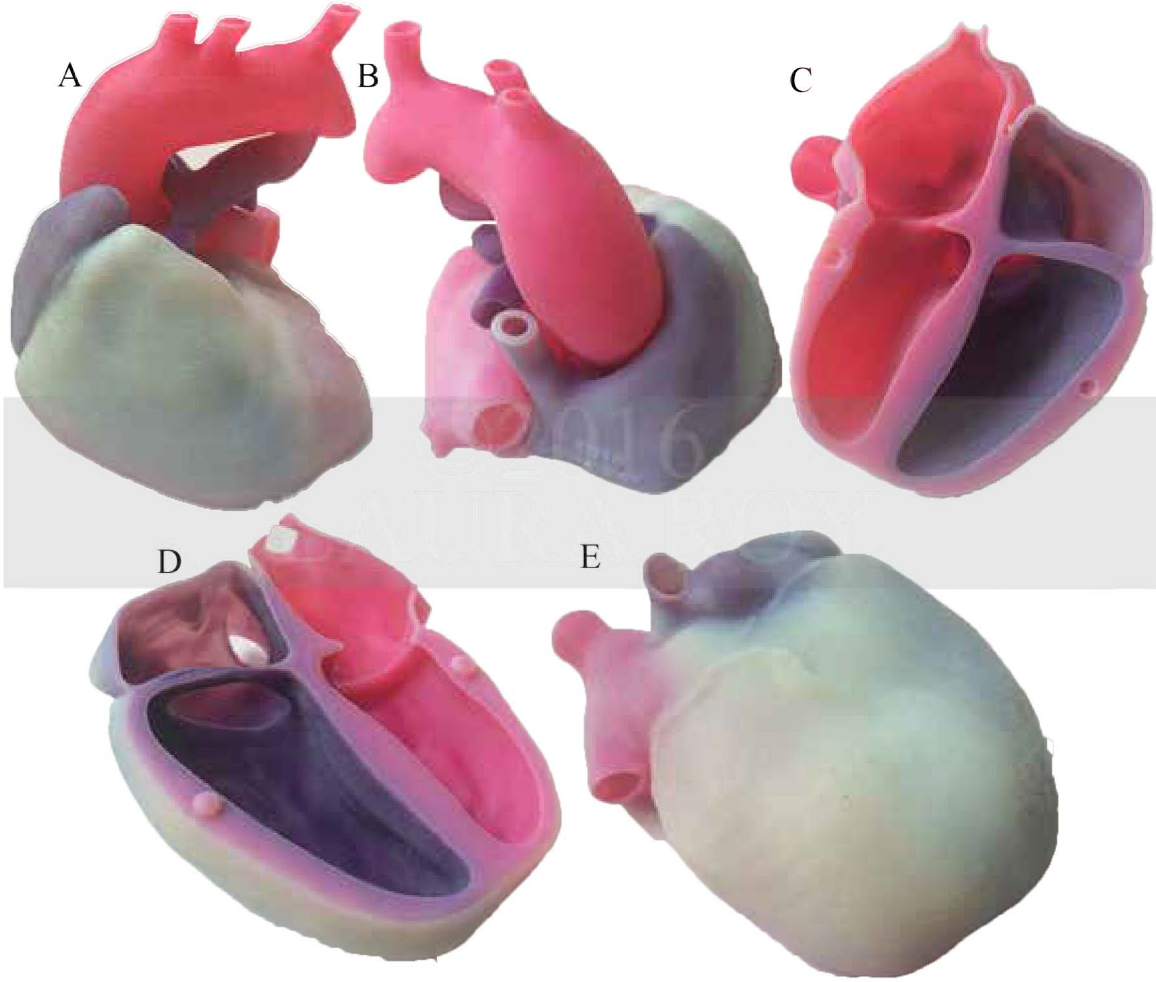

Fig. 3-5: 3D print: Tetralogy of Fallot CHD. Blended color PolyJet print in pure white-cyan-magenta color palette. A: superior from left anterior. B: superior from right posterior. C: superior cross-section. D: inferior cross-section. E: inferior from left posterior.

Fig. 3-6: 3D print: Bespoke base for tetralogy of Fallot CHD. Single color SLS print in white strong and flexible plastic. Left: base alone. Right: base with ColorJet print.

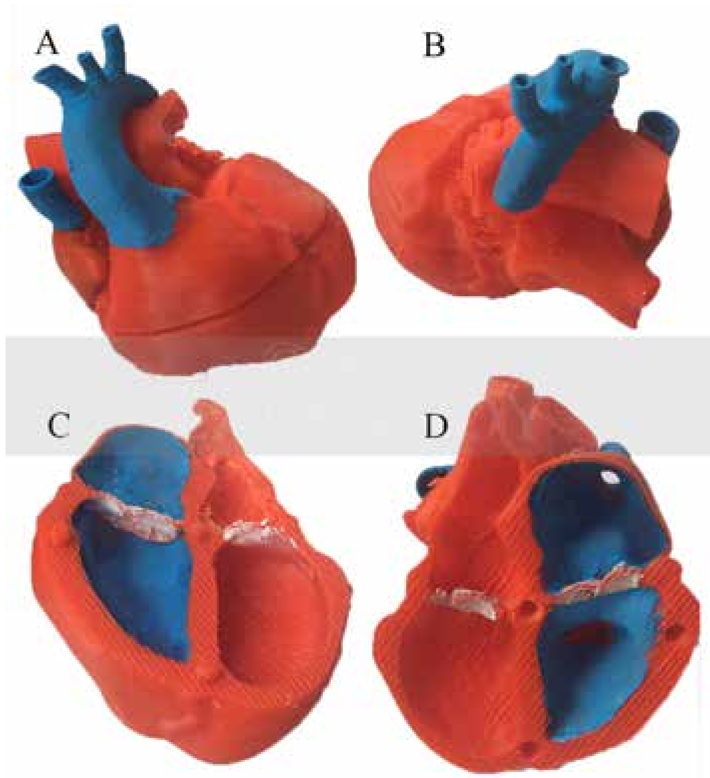

Fig. 3-7: Concept model 3D print: Pre-operative transposition of the great arteries CHD. Single color FFF print using red ABS (0.25mm layer thickness), with the addition of post-printing acrylic spot color. A: anterior. B: posterior. C: inferior cross-section. D: superior cross-section.

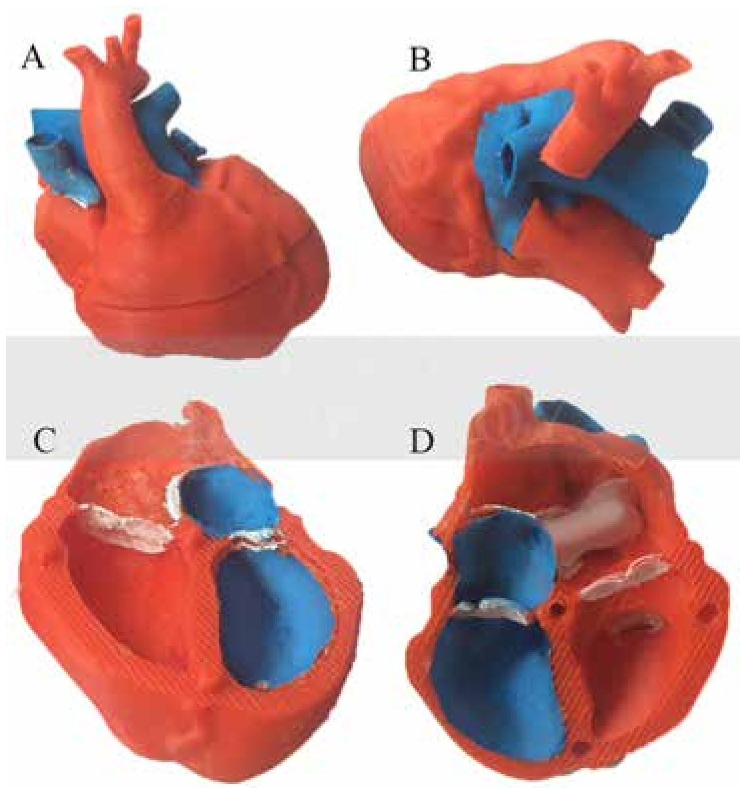

Fig. 3-8: Concept model 3D print: Post-operative (Mustard procedure) transposition of the great arteries CHD. Single color FFF print using red ABS (0.25mm layer thickness), with the addition of post-printing acrylic spot color. A: anterior. B: posterior. C: inferior cross-section. D: superior cross-section.

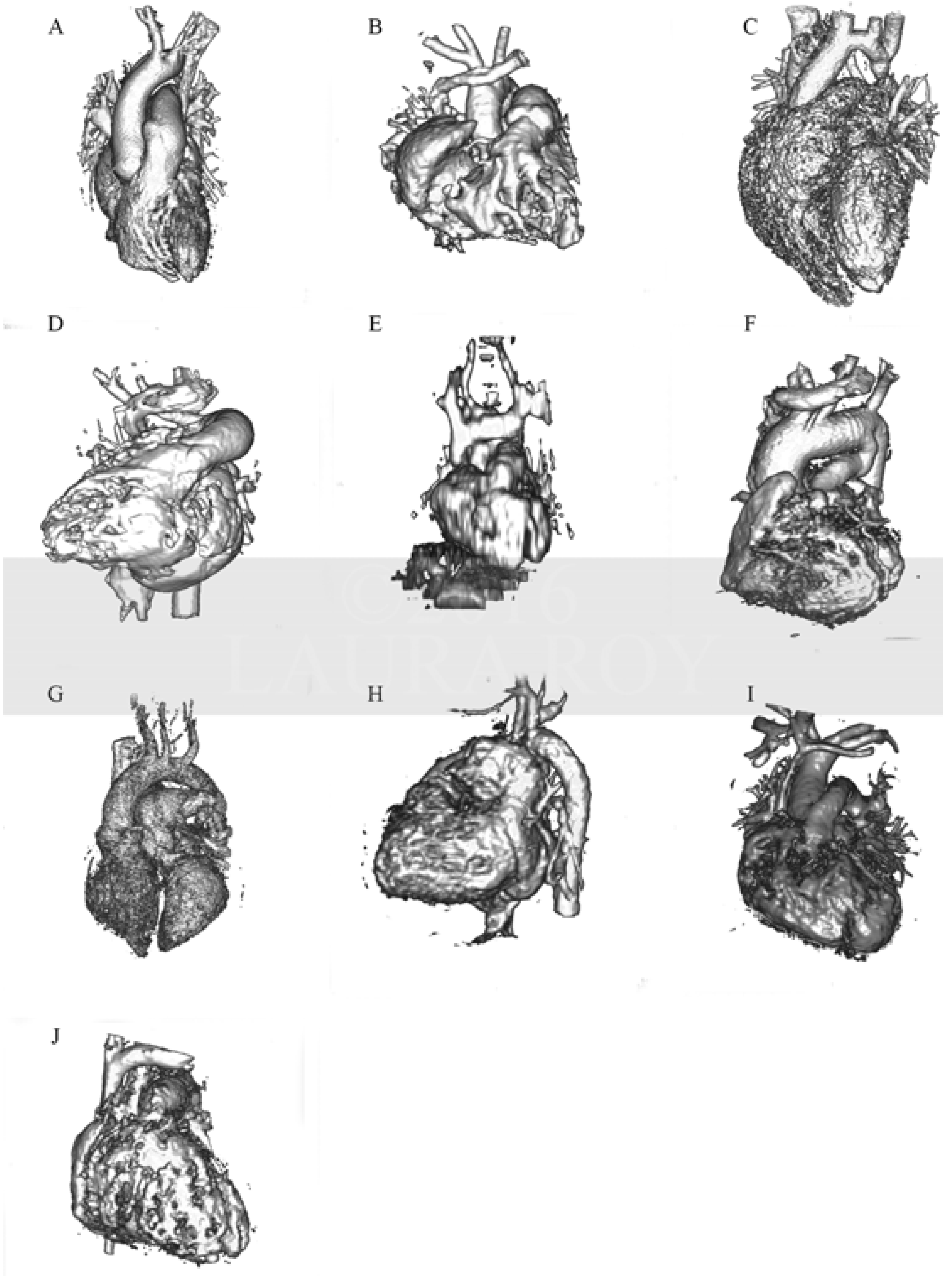

Fig. 3-9: Example screenshots of segmented CHD cardiovascular data. A: Aortic root aneurysm. B: Atrial septal defect. C: Coarctation of the aorta. D: Pulmonic stenosis. E: Total anomalous pulmonary venous return. F: Tetralogy of Fallot. G: Transposition of the great arteries. H: Tricuspid atresia. I: Truncus arteriosus. J: Ventricular septal defect.

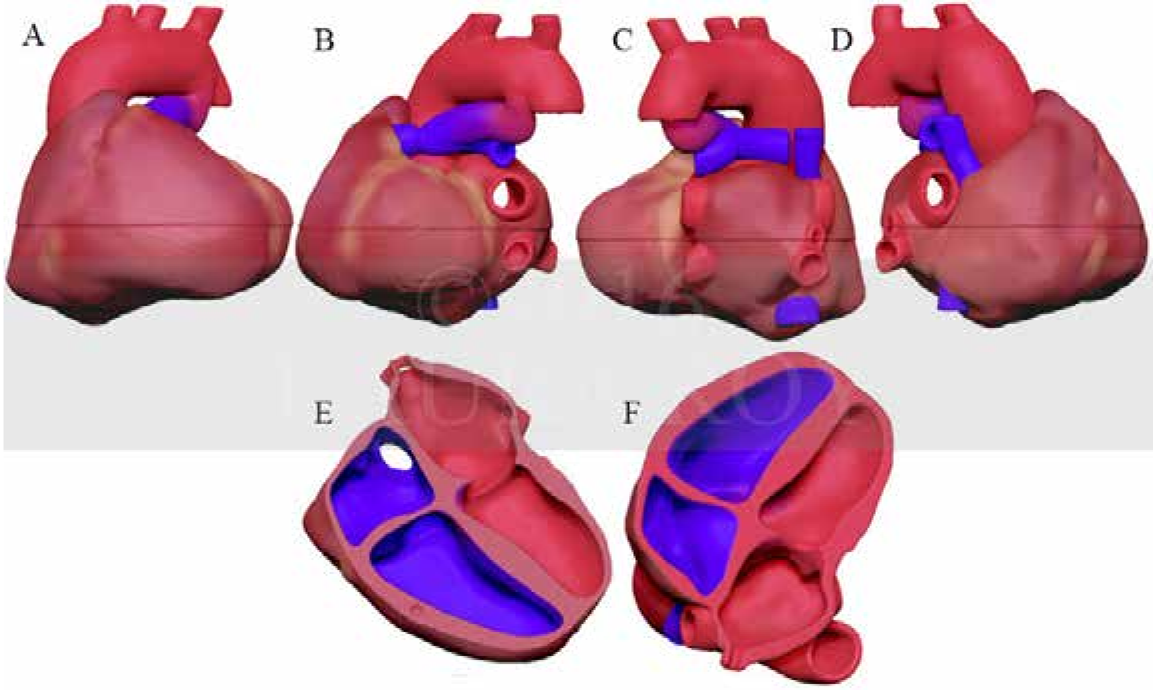

Fig. 3-10: Digital model of Tetralogy of Fallot CHD: A: anterior. B: left. C: posterior. D: right. E: inferior. F: superior.

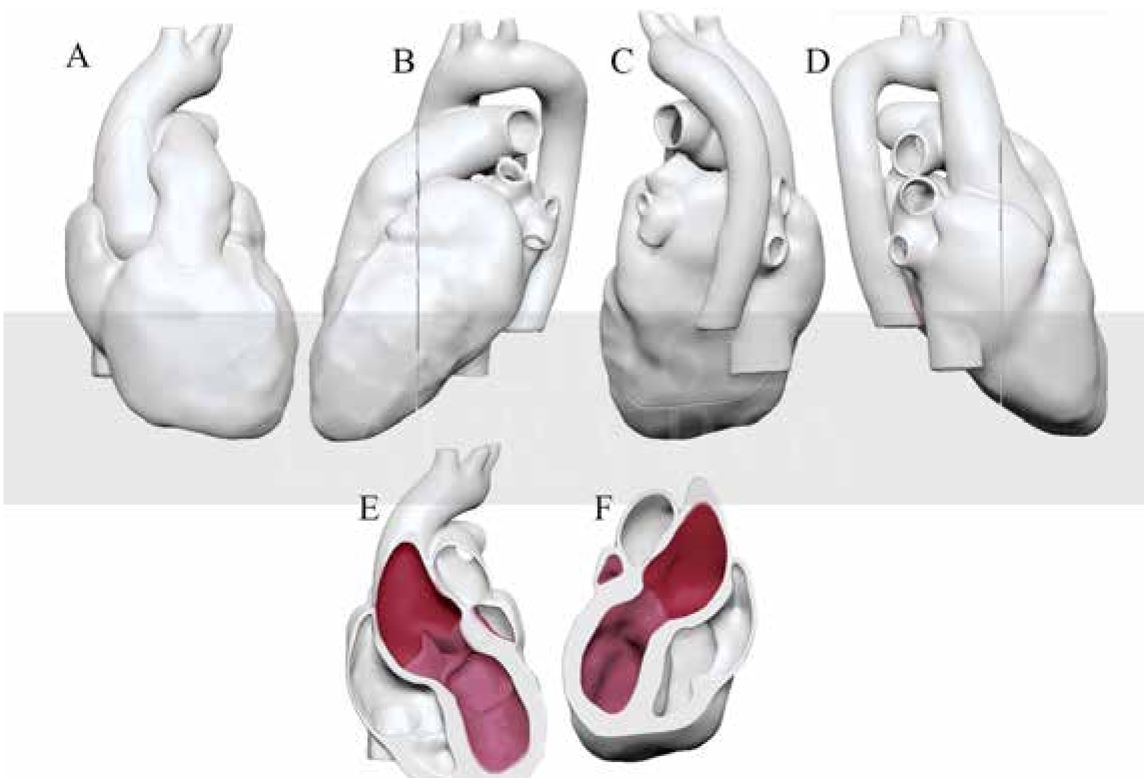

Fig. 3-11: Digital model of pre-operative aortic root aneurysm CHD: A: anterior. B: left. C: posterior. D: right. E: posterior.
F: inferior.

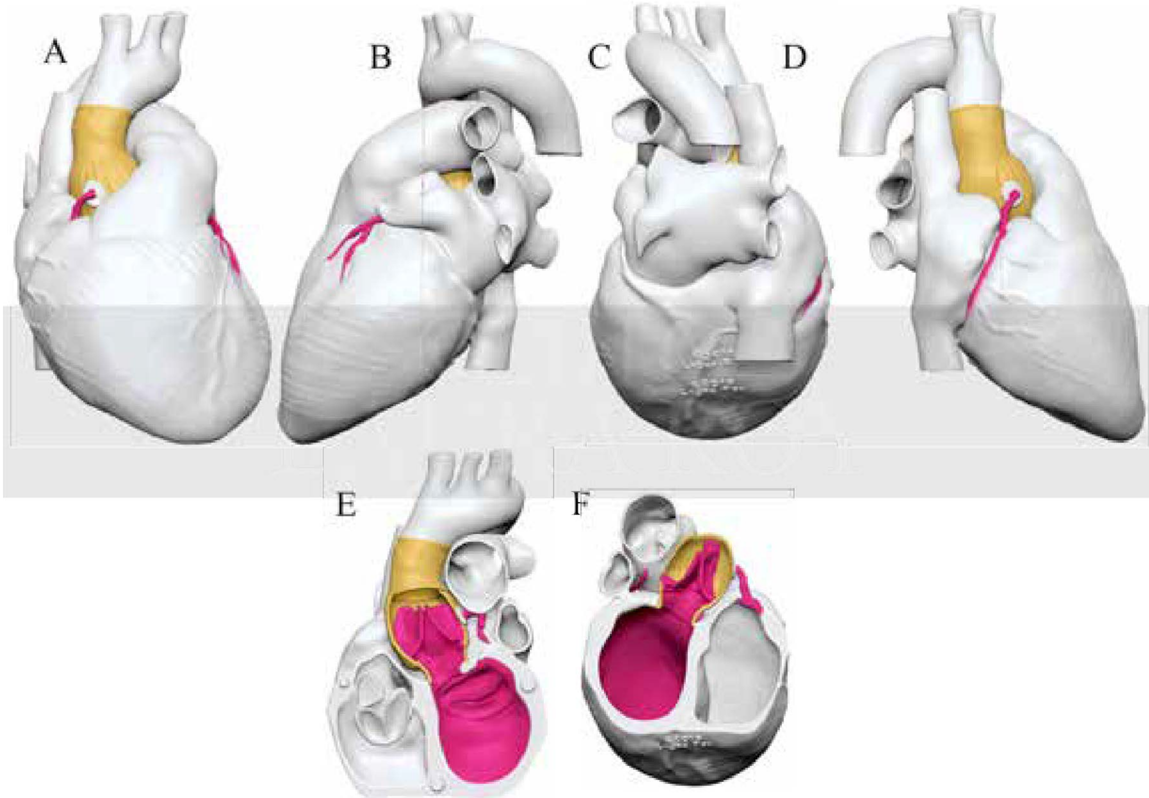

Fig. 3-12: Digital model of post-operative aortic root aneurysm CHD. A: anterior. B: left. C: posterior. D: right. E: posterior. F: inferior.

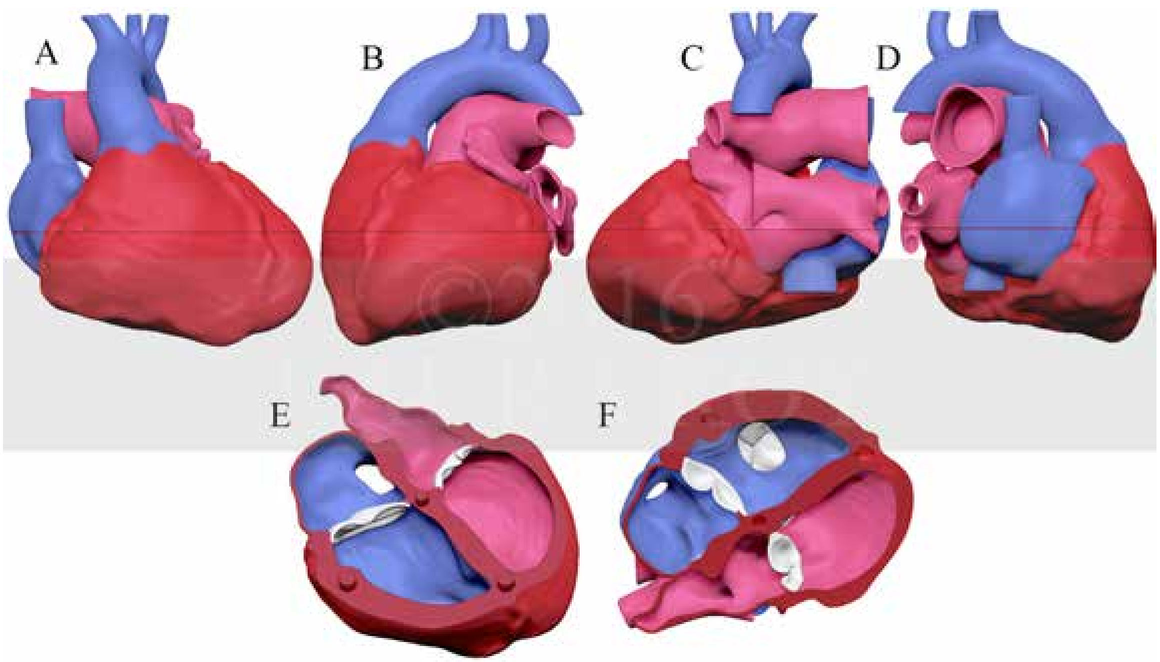

Fig. 3-13: Digital model of pre-operative transposition of the great arteries CHD. A: anterior. B: left. C: posterior. D: right. E: inferior. F: superior.

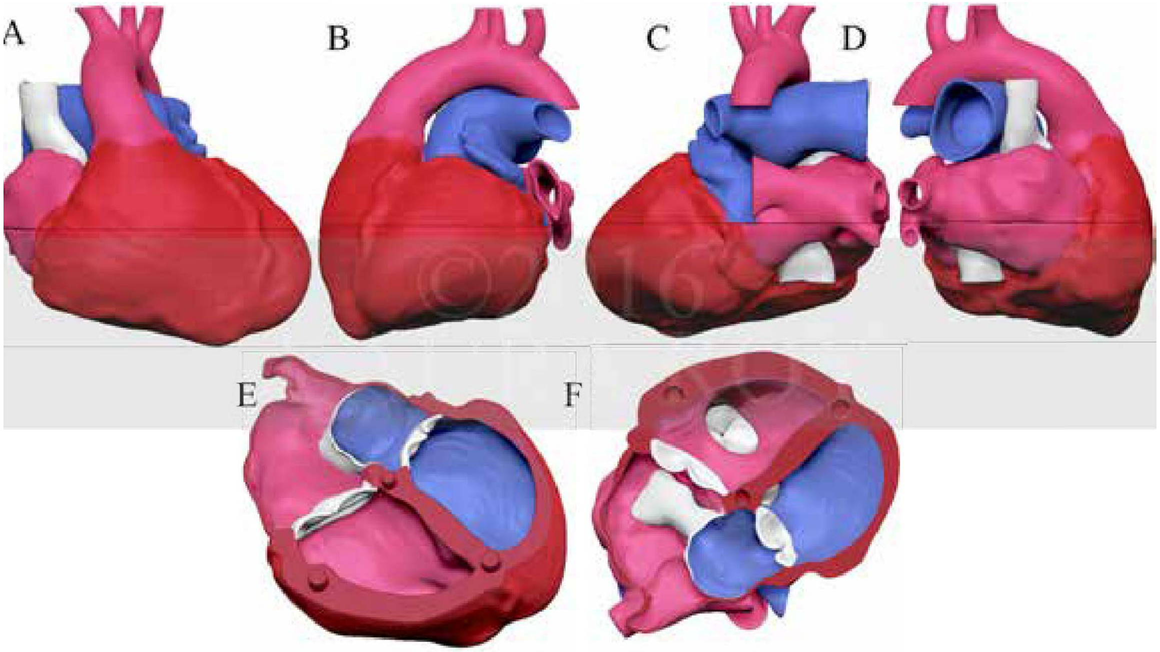

Fig. 3-14: Digital model of post-operative (Mustard) transposition of the great arteries CHD: A: anterior. B: left. C: posterior. D: right. E: inferior. F: superior.

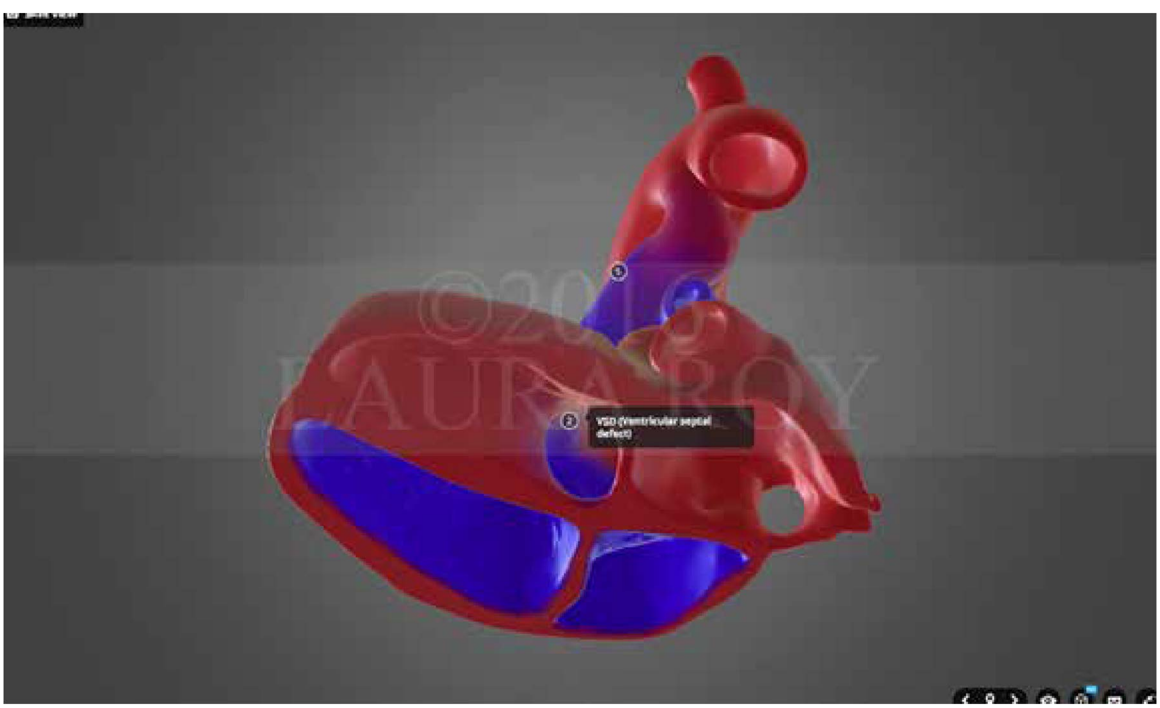

Fig. 3-15: Interactive annotated heart with tetralogy of Fallot CHD using SketchFab (annotation box: “VSD (Ventricular septal defect)”; other text not intended to be read)

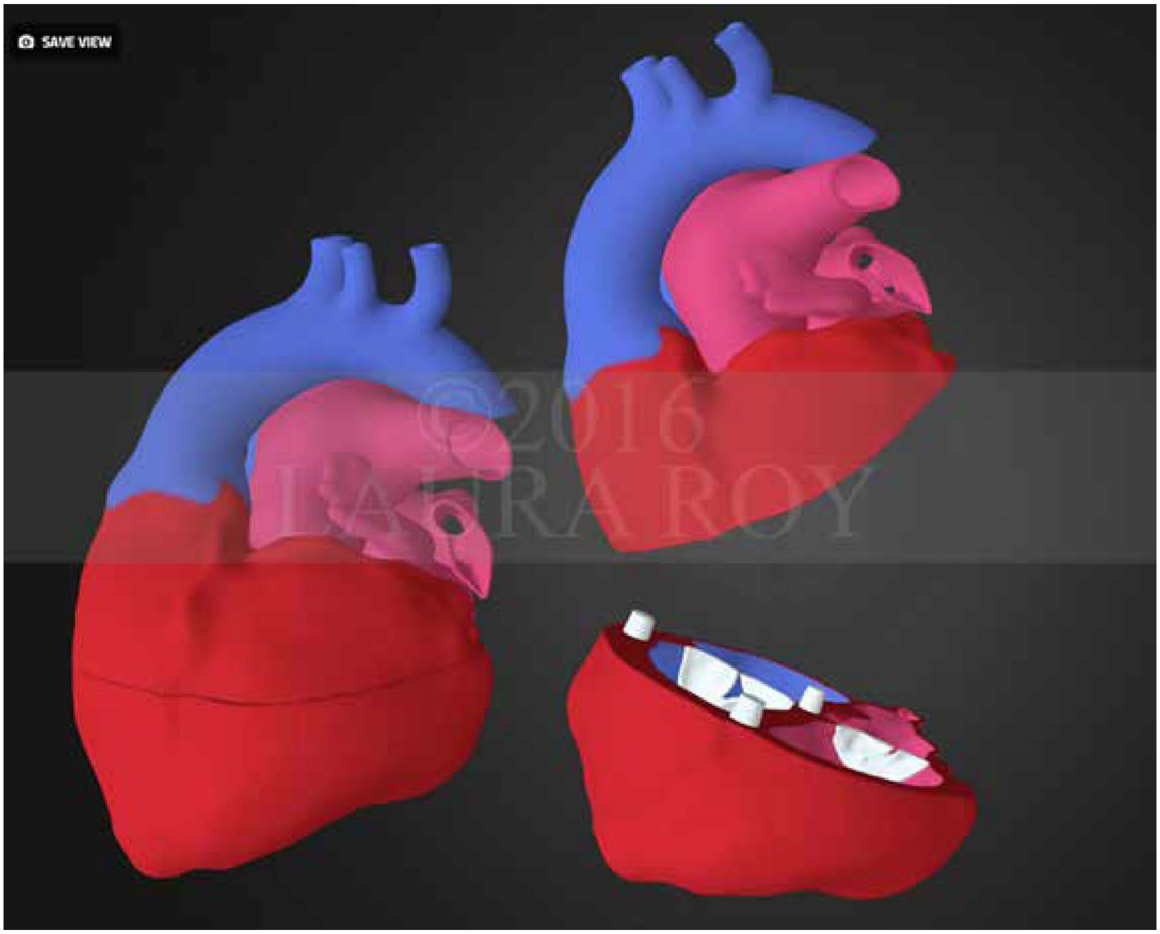

Fig. 3-16: Screenshot of interactive annotated heart with transposition of the great arteries CHD using SketchFab

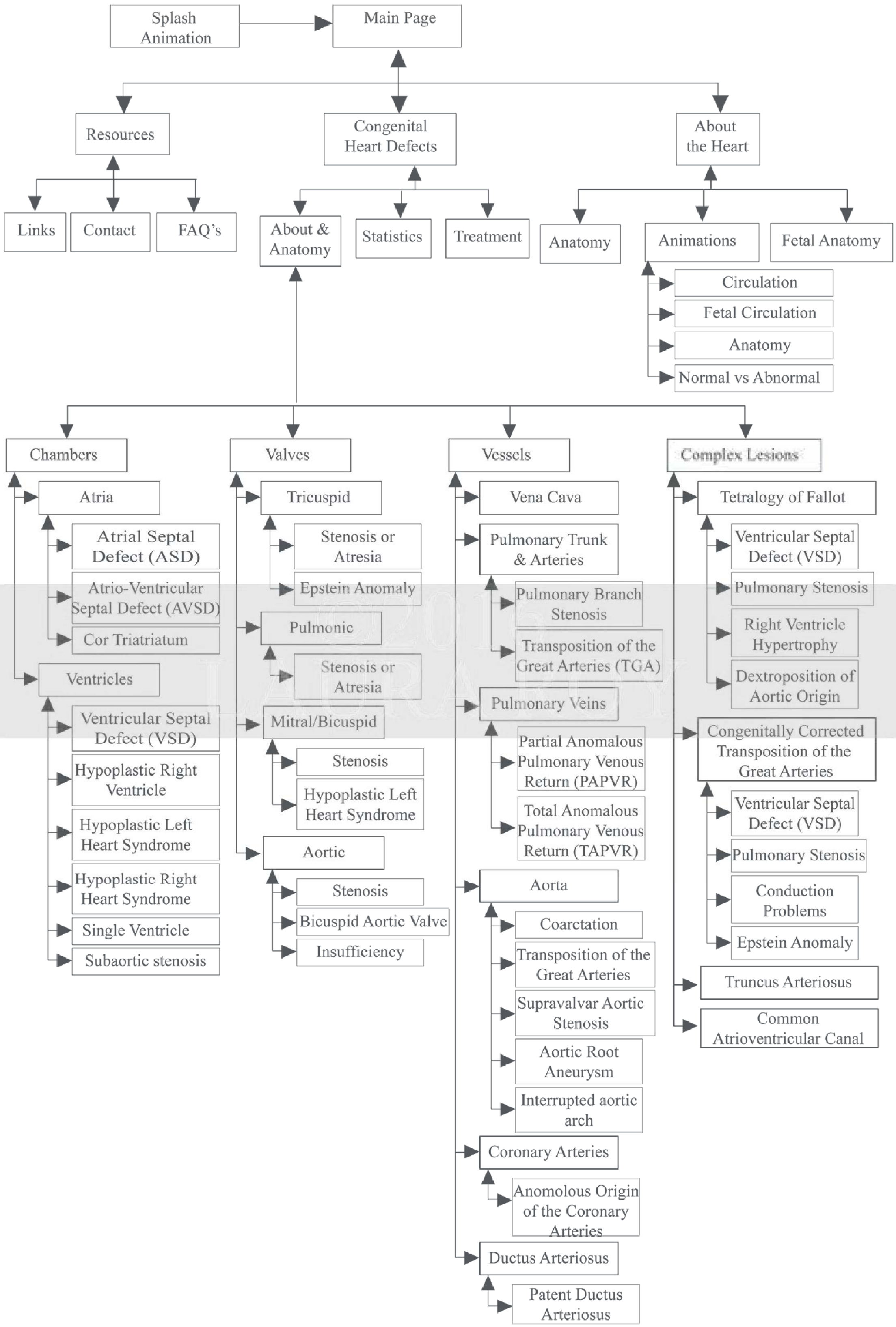

Fig. 3-17: Content flowchart for undeveloped supporting app

ACCESS TO ASSETS

Some tangible assets from this thesis can be viewed at the Department of Art as Applied to Medicine at the Johns Hopkins University School of Medicine. The author can be reached at laura@royillustration.com or via the Department of Art as Applied to Medicine website at www.medicalart.johnshopkins.edu.

Interactive digital models can currently be accessed via SketchFab's website:

- Tetralogy of Fallot: https://skfb.ly/KPSO
- Transposition of the great arteries (pre-operative): https://skfb.ly/LTUI

DISCUSSION

A novel protocol for the production of educational anatomical models produced by 3D printing was developed. It is the first workflow known to the author focused on producing didactic 3D printed models optimized for teaching patients and patient families about CHDs. Of interest is the description of the workflow of printing with Connex3/Adobe technologies that is, to the best of the author's knowledge, the first description in the literature. The author is the first known user external to Stratasys and Adobe to test this new technology.

This research showed that 3D printing allows for the creation of anatomically faithful models with promise for teaching families about CHDs. Materials of various colors, opacities, and color blends were used to investigate optimal teaching qualities. The ability to mimic soft tissue properties was possible with flexible materials.

While this research successfully produced tangible 3D printed cardiovascular models CHDs optimized for teaching, there is room for continued investigation. Future study should include whether 3D printed didactic models translate into short-term and/or long-term CHD understanding among patient families. There should also be research into whether the 3D prints are more, less, or equally successful at teaching when accompanied by 2D and digital 3D resources. The described workflow, techniques, and printing guidelines are also applicable to the production of didactic 3D printed models of other anatomical structures and may be adapted for other audiences to yield educational anatomical models or as alternate didactic resources such as surgical simulators.

DESIGN APPROACH

The current available printing technologies, each with unique material restrictions, dictated the design. Objet Connex3 PolyJet printers were used in this study because of their capability to produce high resolution prints using multiple materials. The Printrbot Simple Metal desktop printer was used for its ability to quickly prototype without waiting for technicians to approve, print, and mail 3D prints. ColorJet technology (Z-Corp printing) was used because it offered the ability to test full color prints. Selective laser sintering with single color strong and flexible plastic was used for detail, durability, and low cost.

Patient data was the basis for design of all the 3D models to accurately represent real anatomy. However, the anatomy was selectively simplified to remove unnecessary detail and to focus attention toward important concepts.

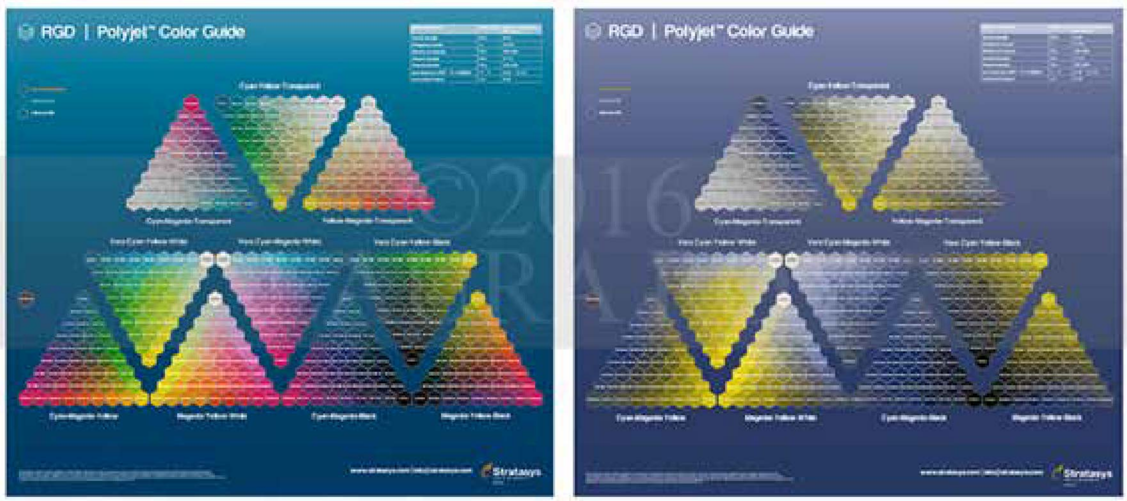

Fig. 4-1: PolyJet colors (Stratasys, 2015) without (left) and with (right) colorblind Protanopia filter (text not intended to be read)

Following anatomical teaching convention, red and blue hues were used to distinguish oxygenated and de-oxygenated blood. The colorblind audience was considered (fig. 4-1) because as many as 8% of males and 0.5% of women of Northern European ancestry are red-green colorblind (National Eye Institute, 2015), causing inability to distinguish between many hues between the blue and red range. This is a particularly salient concern for educational materials relying on the traditional red and blue didactic color-coding, where cyan and magenta can look the same to a colorblind viewer. Because cyan and magenta were used as the main colors for the PolyJet models, values and hues were adjusted slightly to accommodate color-blind users when possible. Guidelines for 3D printed models were further determined on a case-by-case basis. Numerous didactic approaches were considered and can be reviewed in Appendix B.

DIGITAL MODELING PROCESS

CT data sets from patients were used to help ensure anatomical realism of each CHD. High-speed CT was used for scanning because it decreased the likelihood of motion blur and undesirable artifacts. With a low dose of radiation, small children and infants could be scanned without sedation—making it a desirable alternative to MRI. The DICOM file format was used for storage of imaging data because the DICOM file type is widely recognized by medical image viewing software. Use of multiple imaging methods could improve modeling efficiency and realism of future 3D CHD models. Echo in particular would be useful for more accurate valve structures.

Horos, a 64-bit DICOM image viewer with the capability of extracting 3D volumes as surface models, was used for segmentation of structures from the DICOM files. It should be noted that Horos is virtually identical to the program OxiriX MD 64, which is commonly used by biomedical artists. Horos is free but lacks FDA approval, whereas OxiriX currently charges for their 64-bit version that is FDA approved. Segmentation was tested in 3D Slicer, OxiriX, Horos, and InVesalius, each of which are open-source programs based on the freely available Visualization Toolkit from the NIH. Horos and OxiriX were found to have the most robust interface with adequate amounts of relevant OxiriX documentation.

Horos is not as robust as some other programs that have made major advancements in segmentation technology. Using a software with better segmentation capabilities would decrease time spent on segmentation and post-processing of segmented volumes. Mimics®, a program with algorithms developed to segment individual heart cavities and structures, would significantly decrease manual segmentation time and might improve anatomical fidelity. Because software such as Mimics is expensive, costing several thousands of dollars, project scale and audience should be taken into account when choosing which software to use. Enhanced anatomical fidelity would be of greater importance when designing for a medical rather than a lay audience. For the purposes of patient and patient family education, Horos is sufficient.

For cardiovascular segmentation, the scissor tool technique described in the materials and methods section of this thesis was most efficient. Other segmentation workflows were tested and rejected. Although not used for the models produced in this work, they may be useful for segmenting other structures.

One of these, ROIs traced with the pencil tool, was tested. Tracing was most easily achieved by first adjusting the WL/WW, CLUT, and Opacity settings to clearly differentiate boundaries of the traced structure (fig. 4-2). This was repeated for each slice as necessary by copying and pasting the previous ROI and making adjustments with the repulsor tool (fig. 4-3). Defining ROIs with the brush tool was also tested. The eraser setting was used to adjust the brush ROI; otherwise the process was the same as the tracing ROI method. Brush ROIs were found to be less responsive than the tracing/repulsor method and hence took more time. After defining a series of ROIs by tracing or brush, pixel values outside the ROIs were set to -3024 and inside were set to 500. The slices could then be inspected in the 3D Volume Renderer and exported as a surface mesh set to pixel value of 500 via the 3D Surface Renderer.

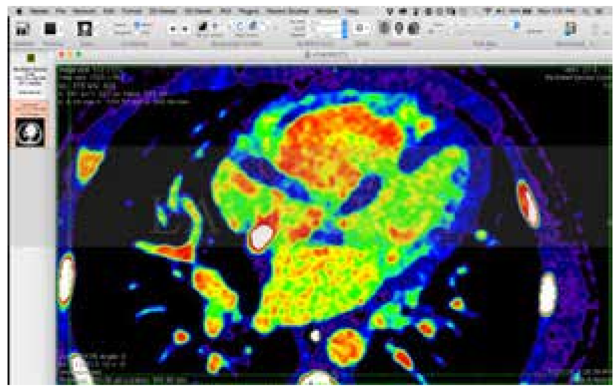

Fig. 4-2: Adjusted CLUT to NIH settings for clarity (text not intended to be read)

The "Generate Missing ROIs" operation was tested with both traced ROIs and brush ROIs. Rather than drawing ROIs on every slice, ROIs were drawn only on intermittent slices. Horos was used to automatically generate the empty slices in between (ROI>ROI Volume>Generate Missing ROIs). These ROI segmentation methods were rejected because they were tedious and time-consuming to get an accurate result. The "Generate Missing ROIs" method was faster but less accurate than manually tracing or brushing ROIs on every layer. Particularly for a complicated, branching structure like the heart, it required tedious readjustment of ROIs to ensure accurate segmentation. These methods also tended to produce visibly stair-stepped meshes. It is possible that using the "Generate Missing ROIs" function with ROIs significantly larger than the desired extraction area would be useful to precede the scissors method.

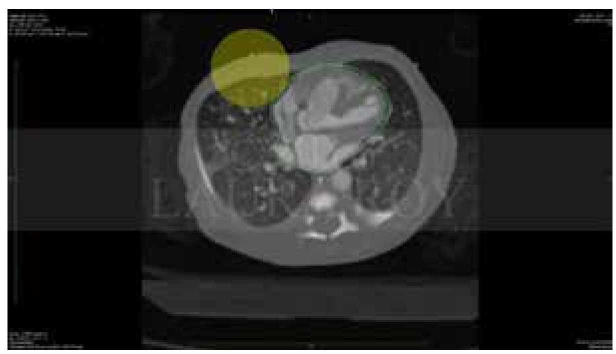

Fig. 4-3: CT image slice with traced ROI (green) being adjusted by repulsor tool (yellow). (Text not intended to be read)

Another strategy, pixel replacement, was used to isolate the heart walls. Pixel values within the heart walls were recorded. For example, in the tetralogy of Fallot data set, the cardiac wall values ranged from about 0-250. Using pixel replacement, the values less than 0 and higher than the 250 were set to -3024 (black). Then, all pixels above -3023 were set to 0. A surface render was produced at 0 pixels and exported as an .obj file to obtain the heart without the inner cavities. This yielded mixed results. It produced an acceptable heart model, however it also captured various other bodily structures that had to be removed in ZBrush. It may be possible to combine this strategy with the scissor tool for future iterations.

After developing an efficient workflow, the time it took the author to segment both inner and outer surfaces of the heart in Horos was about 30-60 minutes. The inner surface of the heart was readily segmented based on the blood volumes. However, even with the high-speed, high-resolution CT, the valves and the cardiac borders were not clearly defined in all of the DICOM sets. Valves had to be reconstructed. Trial and error within the Horos Surface Renderer was necessary to find a true representation of the outer surface and a significant amount of post-processing was necessary before didactic modeling could begin.

Digital models were created in ZBrush by combining segmented inner and outer heart surfaces. ZBrush had both disadvantages and advantages. One disadvantage of ZBrush for this project was the lack of warning response if the 3D Print Exporter ZPlugin was unable to export a subtool. In some cases, ZBrush failed to export a subtool, and no notification of the failure was given to the user. Thus, when exporting multiple .stl files to be recompiled as a single print (as is the case for multi-shell PolyJet printing), it would be easy to miss a shell that had not been exported properly. It is this author’s recommendation that netfabb or another similar program be used to verify that each shell was successfully exported. The reason for the export failure has not been determined; however, duplicating, retopologizing, and projecting detail onto the duplicated shell yielded an exportable shell in the three cases experienced by the author.

Other disadvantages of ZBrush included the lack of clear measurements and grid system coordinates standard in most 3D modeling programs. Polygonal models exist primarily in relative proportion to each other. The inability of ZBrush to close tubes with the cap geometry removed without covering the lumen was another production issue that required careful planning. The tool and subtool hierarchy within ZBrush required much time adjusting settings and visibility, as well as renaming subtools versus the equivalent actions in other 3D modeling programs. The benefits ultimately outweigh the negative aspects, however. ZBrush is capable of managing the large number of polygons necessary for detailed sculpting. Messy retopologization was easy with the DynaMesh function, and clean retopologization was easy with the ZRemesher function. UV map production and PolyPainting models were intuitive. For most non-menu actions, ZBrush was very responsive.

Model production was completed in ZBrush for all models except those printed using the Connex3/Adobe workflow. Painting in Photoshop had several advantages and some disadvantages. The ability to paint texture maps in multiple layers with transparency and blend modes offered a great deal of flexibility and permitted significant detail. Vector masks were also used and could produce sharp, clean edges on texture maps.

Photoshop was ineffective at assessing the complex cardiac models to produce clean UV maps, so each UV map was produced in ZBrush before importing the model into Photoshop. Compared with ZBrush, Photoshop lagged during the painting process with high-polygon models, which is why an attempt to paint partially in ZBrush was tested for some of the Connex3/Adobe models: Colors using the Stratasys color profiles in Photoshop were observed and desired RGB values were recorded, then the model was loosely PolyPainted in ZBrush based on those values. The texture maps were re-exported to replace the texture map in Photoshop for previewing approximate colors and adding detail. To ensure this workflow was not the cause of print previewing issues, a model with a UV map was painted in Photoshop within a Stratasys profile. RGB values were noted and the same model was painted in ZBrush in the same pattern. A texture map produced from the ZBrush model was exported and used to replace the texture map of the Photoshop model. Despite slight changes in color placement, the color appearance within Photoshop remained consistent for both texture maps.

Photoshop workflow efficiency could potentially benefit from integration of bump maps (maps that indicate extra topological detail) in conjunction with retopologized low-polygon models to decrease file size without losing detail. Another workflow recommended by Richard Curtis, Principal Solutions Consult at Adobe (2016a), was to export the least and most subdivided versions of a model from ZBrush and do the majority of Photoshop painting on the lower polygon model. The same texture map could then be applied to the more subdivided model and further detailed as desired. This was successfully tested and is recommended.

Specifically pertaining to the Connex3/Adobe technology, inaccurate color in the 3D printed models was a major production issue. This technology was just released in February 2016, and the author was identified as the first customer to test it via Stratasys Direct. As with any new

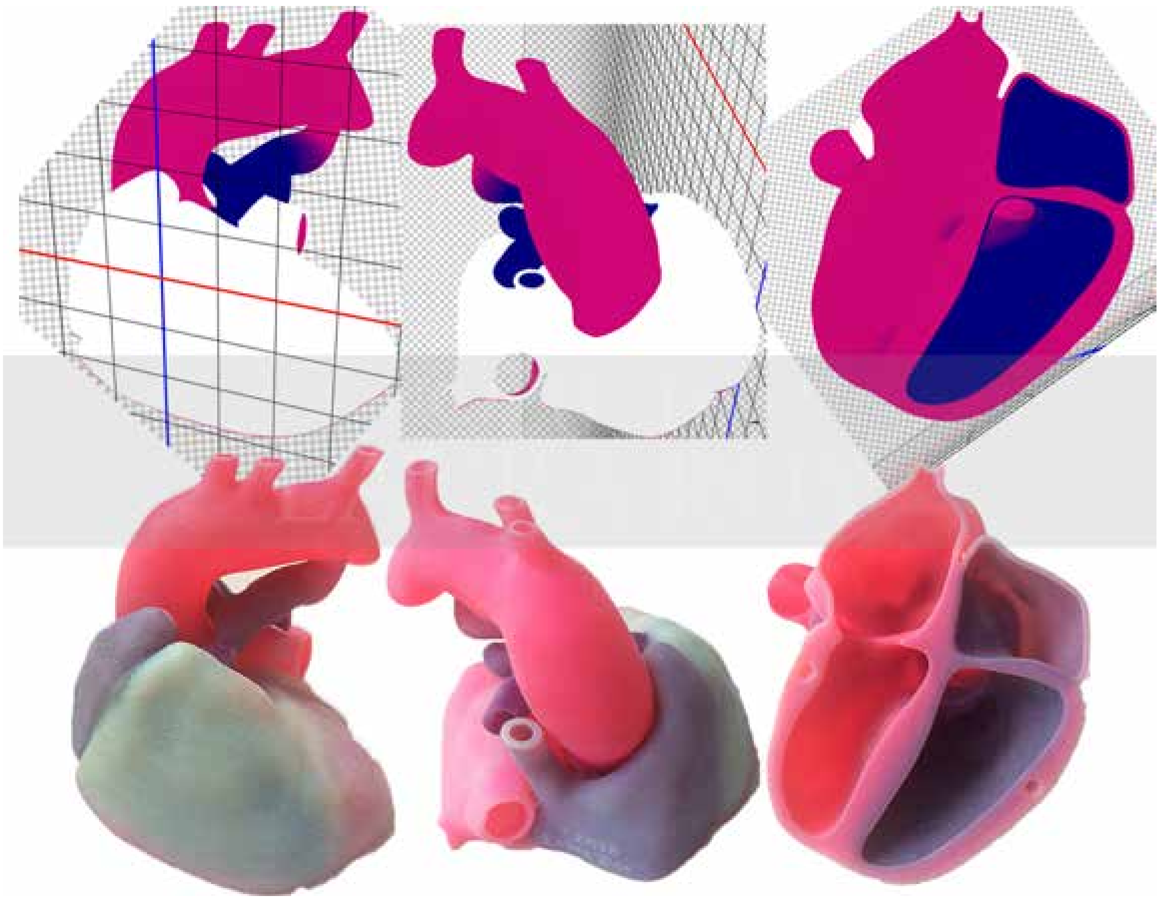

Fig. 4-4: Connex3/Adobe preview issue. Top: Photoshop preview. Bottom: Resulting 3D printed PolyJet model.

technology, there were some technical issues dealing with both inaccurate color previews and undesired color bleed (fig. 4-4).

To varying degrees, print colors did not match colors shown in Photoshop. For example, blue viewed with the cyan-magenta-white profile printed as lavender (fig. 4-4). Gradients from cyan to magenta were not achievable in Photoshop with the Stratasys color profiles. A dark blue (fig. 4-5) was present in all blends between cyan and magenta as opposed to a cyan

Fig. 4-5: Photoshop screenshot showing dark blue band formed when blending cyan and magenta

to violet to magenta gradient. According to Adobe, "The Dark is a symptom of the Cyan clipping out to black [too] early" (Curtis, 2016b). Stratasys Direct Manufacturing confirmed that the dark blue band would print: "It looks like it has a slight gradient starting at the magenta, then a solid purple color than a hard change to blue. That would have to be something it is adjusted in Photoshop, but that would definitely show up on the print," (Stein, 2016a).

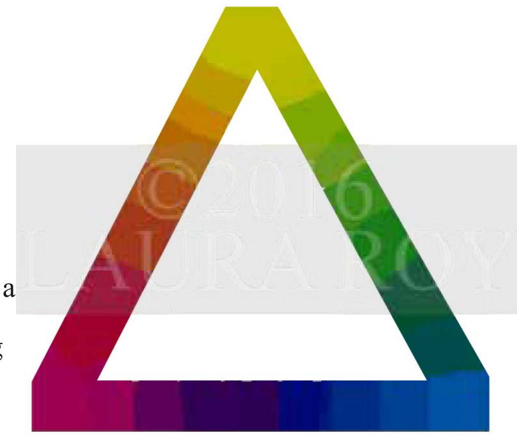

Fig. 4-6: Color triangle produced within the Stratasys cyan-magenta-yellow color profile

The other Connex3/Adobe issue was color bleeding (Fig. 4-4). Walls of the Photoshop PolyJet 3D prints were measured with a calipers to determine a relationship between color bleed and wall thickness. Walls of roughly 1 mm–3 mm exhibited significant color bleeding, walls 4 mm–7 mm showed some color bleeding, while walls 8 mm–10 mm showed minimal color bleeding. No walls thicker than 10 mm were printed for this thesis.

For consistent and reliable results, the color profiles must be reviewed and adjusted by Stratasys and Adobe to prevent the dark blue banding and to correlate screen colors to print colors. It would be useful for Adobe to provide a palette of colors to use with the color picker corresponding to known material blends for each PolyJet palette, like that shown in fig. 4-6.

3D PRINTED MODELS

Cost of model production was highly variable based on printing technique. FFF cost less than a dollar in materials costs for each model. ColorJet cost about $50 per piece ($100 per heart). Cost for outsourcing of PolyJet models on the Connex3 ranged from about $250–$350 per piece ($500–$700 per heart), while the cost to print a bespoke base in SLS was $15–$25.

FFF and SLS prints were the most durable and could be handled without concern about breakage. The flexible PolyJet print was very resilient, while the rigid was slightly more fragile. Particularly in thin-walled areas, both flexible and rigid PolyJet prints were vulnerable to breakage. They were found to have issues with cracking in the walls of small structures with hollow lumens where walls were 1mm thick. In all models, this probably resulted from the pressure-washing step to remove support material after printing. Walls of the same 1 mm thickness toward the edge of the model did not break, so it was likely caused by too much pressure buildup within internal parts of the model. It was recommended by Stratasys to avoid thin walls in those areas and to make internal structures solid when possible (Stein, 2016b). ColorJet prints were the most fragile, although an epoxy resin coat provided additional strength.

Build lines were most visible in FFF prints, slightly visible in ColorJet and PolyJet prints, and barely detectable in SLS prints. FFF prints showed clear build lines and previous support structure points of contact. ColorJet prints showed some Z-stepping but it was largely unnoticeable following the epoxy resin treatment. PolyJet prints exhibited some Z-stepping but it was minimal and required careful attention to identify. Odor associated with prints was also noticeable. The flexible PolyJet print had a strong odor and the rigid Photoshop PolyJet prints had a slight odor. The ColorJet, FFF, and SLS prints had negligible odor. While it has not, to the author's knowledge, been tested, PolyJet prints are probably the easiest to clean and disinfect. Toxicity and disinfectability should be further researched before leaving models with children.

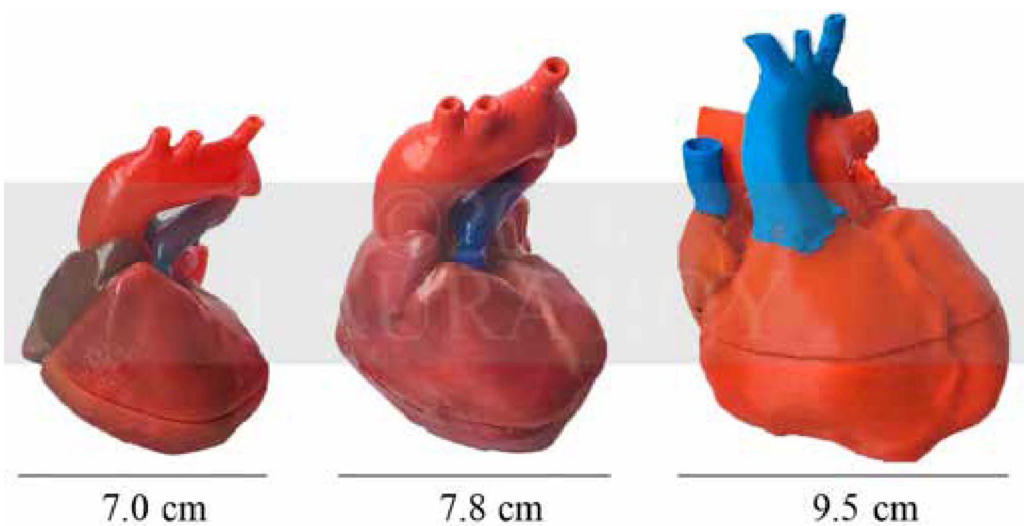

Fig. 4-7: Size range of 3D printed models

Multiple hand-sized 3D printed models were produced (fig. 4-7). A difference of only a centimeter in width resulted in a very different experience and affected the ability to view the anatomy. A size of 7 cm–8 cm was favored by cardiac surgeons and cardiologists to make anatomy clearly visible while still giving the sense that it is a pediatric heart.

INTERACTIVITY FOR A SUPPORTING APP

QuickTime Virtual Reality (QTVR) is a technology used to produce a model or environment viewable from 360º. QTVR was still used regularly by medical illustrators and supported by many 3D software programs until 2015. QTVR is now officially retired and QuickTime recommends that developers explore QTKit and Core Video instead.

Initial plans for this research included use of QTVR as the basis for digital models to be viewed from 360º to supplement the 3D prints. Because QTVR was no longer available, significant additional research was necessary to find a suitable replacement. SketchFab was selected because of its fast rendering capabilities, its ability for the user to fully rotate and zoom into models, the option to annotate models, and the ability to integrate animation. SketchFab requires Internet access, which can be either a limitation or strength. SketchFab can be supplemented by coding, but it does not require it. The procedure described by Roth (2016) to use HTML coding to enhance a SketchFab model with additional interface was tested successfully. This allowed for more controls and additional annotation information. Further exploration of coding with SketchFab is recommended. SketchFab's options far exceed QTVR and make it a superior and more versatile teaching tool. Additional capabilities that would further improve its teaching potential would be the option to hide or reveal parts of the model on demand, to integrate annotations into animations, and to animate transparency. It is possible to do these things in software like Unity, but it requires extra time and expertise. SketchFab is an excellent option for a basic interactive or animated digital 3D model.

FUTURE OBJECTIVES

More research should be done to identify preferences across the range of potential users. In particular, patient families should be consulted to determine interest in color, flexibility, transparency, degree of detail, and use of labels or arrows. A systematic assessment of the didactic efficiency of these variables would be of use. A more rigorous analysis of the educational benefits of 3D models over 2D illustrations for teaching about the spatial aspects of anatomy, including CHDs, should also be performed.

Feedback from consultant pediatric cardiologists, cardiac surgeons, and surgical residents indicated the potential need for additional models with the following design elements. Flexible PolyJet, rigid PolyJet, and ColorJet could be used for 3D printed models. Flexible materials should be used whenever possible and natural heart colors combined with conventional didactic color is preferable. Added labeling and directional arrows may be helpful to indicate blood flow direction. The CHD models should be printed at an average size of 7.5 cm in any direction. Most often a four-chamber cross-section should be used. Grafts and patches should be shown in a unique color and texture from all other parts of the model. For some CHDs, two models with different cross-sections may be desirable. More research should be done with patient families to identify whether structures not relevant to the defect should be included (e.g., valves, coronary arteries), and to what level of detail.

In addition to the 3D printed CHD models, a normal heart should be printed at a variety of sizes (e.g., premature, newborn, toddler, ~4 year old, and teenager). This would allow cardiac surgeons and cardiologists to show parents the approximate size of their child's heart without compromising visibility on the CHD models.

CONCLUSION

Some aspects of the technology explored in this investigation have issues that still need to be worked out, but the results are promising. The Connex3/Adobe technology is capable of producing results unlike any in the history of 3D printing. While ColorJet and laminated object manufacturing are capable of producing gradients and full color prints, neither is waterproof nor capable of the resolution offered by PolyJet printing. When the last few issues are worked out with this technology, it will be a powerful tool for producing 3D printed models for many educational purposes. The Connex3/Adobe technology also has potential for clinical and research purposes as additional materials are developed, e.g., the ability to print a gradient with fluorescent or radio-opaque material. Advancements in 3D printing that will significantly aid in didactic development include the ability of PolyJet technology to use more than three materials and to have the option for any color material to be flexible, rigid, opaque, or transparent.

The 3D printed CHD models produced with the other printing technologies were also excellent. PolyJet and ColorJet both have the potential to serve as final models in terms of durability. For prints that will be regularly handled by small children, PolyJet prints are the best choice as they combine detail and color, and are not overly fragile.

This workflow could be adapted for producing models to educate a medical audience such as medical students and surgical residents. For those audiences, style adjustments should be made based on focus group feedback, such as adding detail, printing at life size, using only flexible materials, and limiting color. The workflow can also be adapted to other anatomical structures such as the cerebral vasculature or the hepatic portal system for either a patient or medical audience.

The novel workflow and 3D printed heart models produced within the scope of this project can serve to guide product development of future models to teach anatomy of CHDs to families of afflicted patients. The models provide views into hearts that are truthful to reality and can aid cardiologists and cardiac surgeons in the teaching process to a degree that 2D resources cannot. Truly, a heart in the hand is worth more than two on a page.

APPENDIX A: CONGENITAL HEART DEFECTS

- Absent Pulmonary Valve
- Anomalous Left Coronary Artery
- Aortic Stenosis
- Aortic Valve Stenosis (AVS)
- Aortopulmonary Window
- Atrial Septal Defect (ASD)
- Atrioventricular Canal Defect
- Atrioventricular Septal Defect
- Bicuspid Aortic Valve
- Coarctation of the Aorta
- Complete Congenital Heart Block
- Congenitally Corrected Transposition of the Great Arteries or Great Vessels
- Coronary Artery Anomaly
- Coronary Artery Fistula
- D-Transposition of the great arteries
- Double Chamber Right Ventricle (DCRV)
- Dextrocardia
- DiGeorge syndrome
- Dilated Cardiomyopathy
- Double Aortic Arch
- Double Inlet Left Ventricle
- Double Outlet Right Ventricle
- Down syndrome
- Ebstein anomaly
- Eisenmenger Complex
- Endocardial Cushion Defect
- Endocardial Fibroelastosis
- Holt-Oram syndrome
- Hypertension, Pulmonary
- Hypertension, Systemic
- Hypertrophic Cardiomyopathy
- Hypoplastic left heart
- Hypoplastic Left Heart Syndrome
- Hypoplastic Right Heart syndrome

- I-transposition of the great arteries
- Interrupted Aortic Arch
- Isolated Non-Compaction of Left Ventricular Myocardium
- Kawasaki Disease
- Left Ventricular Outflow Tract Obstruction
- levo-Transposition of the great arteries (l-TGA)
- Long QT syndrome
- Major Aorta/Pulmonary Collateral Arteries
- Marfan syndrome
- Mitral Stenosis
- Mitral Valve Prolapse
- Myocarditis
- Noonan syndrome
- Partial anomalous pulmonary venous connection (PAPVC)
- Patent Ductus Arteriosus
- Patent Foramen Ovale
- Pentalogy of Cantrell
- Persistent truncus arteriosus
- Pulmonary Atresia
- Pulmonary Stenosis
- Right Ventricular Outflow Tract Obstruction
- Scimitar syndrome (SS)
- Shone's syndrome/ Shone's complex / Shone's anomaly
- Single Ventricle
- Tetralogy of Fallot
- Total Anomalous Pulmonary Venous Connection (TAPVC)
- Transposition of the Great Arteries or Vessels
- Tricuspid Atresia
- Trisomy 13
- Truncus Arteriosus
- Turner syndrome
- Williams syndrome
- Wolff-Parkinson-White syndrome (WPW)

APPENDIX B: CONCEPT IDEAS

COLOR AND OPACITY

- Spot color on areas of interest, transparent elsewhere
- Swirled, interlocking transparent color shells to show blood shunting
- Color by blood flow
- Clear to indicate absence/atresia (e.g., for tricuspid atresia)
- Color code for normal vs abnormal (e.g., violet versus yellow)
- Normal transparent, abnormal opaque
- Small shells increasing in color intensity approaching the defect (gradient effect)
- Opaque everywhere except for strategically-placed transparent sections to show interior defect(s)

MATERIAL

- Rigid interior and transparent flexible outer (flexibility for texture aesthetic)
- Compare two states in same model (e.g., opaque for abnormal, transparent for normal)
- Flexible everywhere except defect
- Flexible everywhere
- Rigid everywhere

SYMBOL/TEXT/PATTERN USAGE

- Arrows woven through to indicate blood flow
- Directional arrows embedded in walls
- Text labels doubling as arrows to indicate blood flow (could compare normal/abnormal)
- Text labels embedded or embossed (could be raised from interior to maintain smooth exterior texture), or numbers/letters (with legend on back or stand)
- Band/line use to mark edges
- Define areas of interest with pattern/texture

MECHANISM/MODELING APPROACH

- Articulated valves
- Fully print only the abnormal area, vignetting out to a sparse wireframe of the rest of the heart
- 2d wireframe outline (single plane) with 3d defect
- Didactic LED lights
- Rigid base/stand (could suggest adjacent or relevant body parts)

- Simultaneously compare volume/morphology of normal (or corrected) vs abnormal in one model (e.g. pulmonary stenosis or aneurysm). Use color, graphics, to differentiate
- One base heart wireframe with interchangeable pieces for various defects—may take the form of a more schematic illustration or educational toy
- One print that can open into 2+ -sections
- Hinged
- Pegged or ridged
- Slinky/spring opening technique for part or all of model
- Dynamic section boundaries (e.g., one side protruding)
- One print with a hinged hatch to view into a defect.
- Interlocking heart pieces to form puzzle
- Fluid contained within model
- Rigid external arrows to show inflow/outflow; extend beyond great vessels (with labels to, from...)
- Metaphor for flow/inflow/outflow (e.g., faucet, piping, pump)

WORKS CITED

3ders.org. 2015a. "Stratasys 3D Printed Vascular Model Assists Life-Saving Brain Aneurysm Surgery." 3ders.org. November 24. http://www.3ders.org/articles/20151124-stratasys-3d-printed-vascular-model-assists-life-saving-brain-aneurysm-surgery.html.

3ders.org. 2015b. "India's Pediatric Surgeons Turn to 3D Printing for Complex Cardiac Operations." 3ders.org. November 24. http://www.3ders.org/articles/20151124-indias-pediatric-surgeons-turn-to-3d-printing-for-complex-cardiac-operations.html.

3ders.org. 2015c. "Canadian Surgeon Uses 3D Printed Realistic Brain Model to Assist Complex Brain Surgery." 3ders.org. November 11. http://www.3ders.org/articles/20151111-canadian-surgeon-3d-printed-realistic-brain-model-complex-brain-surgery.html.

3ders.org. 2016. "Japanese Medical Insurance to Cover Cost of 3D Printed Organ Models." 3ders.org. January 27. http://www.3ders.org/articles/20160127-japanese-medical-insurance-to-cover-cost-of-3d-printed-organ-models.html.

3dprintingfromscratch.com. 2016a. "Sciaky Announced First Sale of Giant Metal 3D Printer | 3D Printing from Scratch." Accessed February 28. http://3dprintingfromscratch.com/2014/08/sciaky-announced-first-sale-of-giant-metal-3d-printer/.

3dprintingfromscratch.com. 2016b. "Types of 3D Printers or 3D Printing Technologies Overview | 3D Printing from Scratch." Accessed February 28. http://3dprintingfromscratch.com/common/types-of-3d-printers-or-3d-printing-technologies-overview/.

Adam,Rouilly Ltd. 2010. "Series of Models Representing Congenital Heart Defects : Simulators, Anatomical Models and Charts for Clinical Skills, Medical Education and Training." Adam,Rouilly. http://www.adam-rouilly.co.uk/productdetails.aspx?pid=1981&cid=209.

Ars Medica Italia. 2012. "The Multimedia Atlas of Congenital Heart Disease." http://www.arsmedicaitalia.it/?page_id=148&lang=en

Bernhard, Jean-Christophe, Shuji Isotani, Toru Matsugasumi, Vinay Duddalwar, Andrew J. Hung, Evren Suer, Eduard Baco, et al. 2016. "Personalized 3D Printed Model of Kidney and Tumor Anatomy: A Useful Tool for Patient Education." World Journal of Urology 34 (3): 337-45.

Biglino, Giovanni, Claudio Capelli, Jo Wray, Silvia Schievano, Lindsay-Kay Leaver, Sachin Khambadkone, Alessandro Giardini, Graham Derrick, Alexander Jones, and Andrew M. Taylor. 2015. "3D-Manufactured Patient-Specific Models of Congenital Heart Defects for Communication in Clinical Practice: Feasibility and Acceptability." BMJ Open 5 (4): e007165.

Coakley Meghan F., Hurt Darrell E., Weber Nick, Mtingwa Makazi, Fincher Erin C., Alekseyev Vsevelod, Chen David T., et al. 2014. "The NIH 3D Print Exchange: A Public Resource for Bioscientific and Biomedical 3D Prints." 3D Printing and Additive Manufacturing 1 (3). online.liebertpub.com: 137-40.

CDC. 2016a, "Data and Statistics | Congenital Heart Defects." Accessed March 3. http://www.cdc.gov/ncbddd/heartdefects/data.html.

CDC. 2016b. "Key Findings: Prenatal Diagnosis of Congenital Heart Defects." Accessed February 28. http://www.cdc.gov/ncbddd/heartdefects/features/prenatal-diagnosis.html.

Cincinnati Children's Hospital. 2015. "Heartpedia." Version: 1.3.1. App Store. October 28. https://itunes.apple.com/us/app/heartpedia/id885512669.

Clark, S. M., and M. S. Miles. 1999. "Conflicting Responses: The Experiences of Fathers of Infants Diagnfosed with Severe Congenital Heart Disease." Journal of the Society of Pediatric Nurses: JSPN 4 (1): 7-14.

Curtis, Richard. Conversation with Laura Roy. 2016a, February 26.

Curtis, Richard. Email letter to Laura Roy. 2016b, March 8.

Dahku Creations. 2015. “3D Road Map to Congenital Heart Disease.” Version 2.0. App Store. November 11. https://itunes.apple.com/us/app/3d-road-map-to-congenital/id806514218?ls=1.

Kramer, Gerri Freid, and Shari Maurer. 2001. The Parent’s Guide to Children’s Congenital Heart Defects: What They Are, How to Treat Them, How to Cope with Them. Three Rivers Press.

Lim, Kah Heng Alexander, Zhou Yaw Loo, Stephen J. Goldie, Justin W. Adams, and Paul G. McMenamin. 2015. “Use of 3D Printed Models in Medical Education: A Randomized Control Trial Comparing 3D Prints versus Cadaveric Materials for Learning External Cardiac Anatomy.” Anatomical Sciences Education, October. doi:10.1002/ase.1573.

Materialise. 2015. “HeartPrint®: 3D Printing Services for Cardiovascular Anatomy.” http://biomedical.materialise.com/sites/default/files/public/BME/Cardiovascular/AM%20Models/heartprint_catalog.pdf.

Marsden, Alison L., and Jeffrey A. Feinstein. 2015. “Computational Modeling and Engineering in Pediatric and Congenital Heart Disease.” Current Opinion in Pediatrics 27 (5): 587-96.

Mcor Technologies. 2016. “3D Printing and Rapid Prototyping | Mcor Technologies.” 2016. Mcor Technologies. Accessed March 21. http://mcortechnologies.com/.

McMenamin, Paul G., Michelle R. Quayle, Colin R. McHenry, and Justin W. Adams. 2014. “The Production of Anatomical Teaching Resources Using Three-Dimensional (3D) Printing Technology.” Anatomical Sciences Education 7 (6): 479-86.

National Eye Institute. “Facts About Color Blindness.” 2015. National Eye Institute. February. https://nei.nih.gov/health/color_blindness/facts_about.

Neill, Catherine A., Edward B. Clark, and Carleen Clark. 2003. The Heart of a Child: What Families Need to Know about Heart Disorders in Children. JHU Press.

NIH 3D Print Exchange. 2016. “Submission Process.” NIH 3D Print Exchange. Accessed March 1. http://3dprint.nih.gov/collections/heart-library/submission.

Nguyen, N., A. J. Nelson, and T. D. Wilson. 2012. “Computer Visualizations: Factors That Influence Spatial Anatomy Comprehension.” Anatomical Sciences Education. Wiley Online Library. http://onlinelibrary.wiley.com/doi/10.1002/ase.1258/full.

Noel, Cory, and Dr Mark B. Lewin. 2012. “Left to Right Shunt Lesions.” In Textbook of Clinical Pediatrics, 2295-2308. Springer Berlin Heidelberg.

O’Reilly, Michael K., Sven Reese, Therese Herlihy, Tony Geoghegan, Colin P. Cantwell, Robin N. M. Feeney, and James F. X. Jones. 2016. “Fabrication and Assessment of 3D Printed Anatomical Models of the Lower Limb for Anatomical Teaching and Femoral Vessel Access Training in Medicine.” Anatomical Sciences Education 9 (1). Wiley Online Library: 71-79.

PLANFAB. 2015. “Optimize Your Colors for Full Color Sandstone.” PLANFAB. February 2. http://www.planfab.eu/optimize-colors-full-color-sandstone/.

Preece, Daniel, Sarah B. Williams, Richard Lam, and Renate Weller. 2013. “’Let’s Get Physical’: Advantages of a Physical Model over 3D Computer Models and Textbooks in Learning Imaging Anatomy.” Anatomical Sciences Education 6 (4): 216-24.

Pye, Sherry, and Angela Green. 2003. “Parent Education after Newborn Congenital Heart Surgery.” Advances in Neonatal Care: Official Journal of the National Association of Neonatal Nurses 3 (3): 147-56.

RNCeus. 2016. “Normal Vital Signs.” RN Ceus. Accessed March 19. http://www.rnceus.com/psvt/psvtvs.html.

Roth, Mieke. 2016. “How to Make a Real 3D Model Application with.” Sketchfab Blog. March 1. http://blog.sketchfab.com/post/140275769109/how-to-make-a-real-3d-model-application-with.

Schultz, Amy H. 2012. “Obstructive Cardiac Lesions.” In Textbook of Clinical Pediatrics, 2331-

46. Springer Berlin Heidelberg.

Seslar, Stephen P. 2012. “Cyanotic Heart Disease.” In Textbook of Clinical Pediatrics, 2309-30. Springer Berlin Heidelberg.

Shors, Tracey J. 2004. “Learning during Stressful Times.” Learning & Memory 11 (2): 137-44.

Skilton, Michael R., Nick Evans, Kaye A. Griffiths, Jason A. Harmer, and David S. Celermajer. 2005. “Aortic Wall Thickness in Newborns with Intrauterine Growth Restriction.” The Lancet 365 (9469): 1484-86.

Smith, Mark, Colin Newey, Madeline Jones, and Jeff Martin. 2011. “Congenital Heart Disease and Its Effects on Children and Their Families.” Paediatric Nursing 23 (2): 30-35.

Stein, Curtis. Email letter to Laura Roy. 2016a, March 8.

Stein, Curtis. Conversation with Laura Roy. 2016b, March 16.

St. Michael’s. 2016. “CT (CAT) Scan.” Medical Imaging. http://www.stmichaelshospital.com/programs/imaging/ctscan/faq.php.

Stratasys. 2015. “PolyJet Color Materials.” http://usglobalimages.stratasys.com/Main/Files/Material_Spec_Sheets/MSS_PJ_PJColorMaterials.pdf?v=635785241190888627.

Sun, Z., and A. Squelch. 2015. “3D Printed Models of Complex Anatomy in Cardiovascular Disease.” Treatment of Cardiac Hemochromatosis 2 (3): 103-8.

University College London. 1999-2016. “Library of 3D Anatomies.” University College London Clinical Cardiovascular Engineering. http://www.ucl.ac.uk/cardiac-engineering/researchlibrary-of-3d-anatomies.

VITA

Laura was born in Minneapolis, Minnesota. She spent her childhood in Muscatine, Iowa, before moving to Ames in central Iowa where she graduated from Ames High School. Laura attended Iowa State University where she studied a variety of subjects. Laura was inducted into Phi Beta Kappa in 2007. She earned Bachelor of Arts degrees both in Philosophy and in Art & Design, with a French minor, and graduated *magna cum laude* with honors in 2008. It was at Iowa State that Laura first learned of the medical illustration profession. However, inspired by her love for the combination of art, science, and storytelling in food and wine, Laura proceeded to attend the Iowa Culinary Institute to attain an Associates of Applied Sciences degree in Culinary Arts along with a Certificate in Enology.

Laura and her partner Jeremy embarked on a series of adventures including working as cellar and laboratory techs in wineries in New Zealand and Oregon. Captivated by the challenge and reward of scientific and medical illustration, Laura and Jeremy decided to study biological illustration and fine art at Iowa State University. Laura graduated again from Iowa State University *magna cum laude* with honors with a Bachelors of Arts in Biological/Pre-Medical Illustration in 2014 before beginning her studies at the Johns Hopkins University School of Medicine, Department of Art as Applied to Medicine. Laura enjoys telling stories using 3D imagery and realism, and has continued to push beyond the 2D page in this Master's thesis, which brought learning into the tangible 3D realm.

After receiving the degree of Master of Arts in Medical and Biological Illustration in May of 2016, Laura will pursue her career in the field of medical illustration.